

# A Predictive Decision Aid Methodology for Dynamic Mitigation of Influenza Pandemics

**Andrés Uribe-Sánchez**

**Alex Savachkin**

**Tapas K. Das**

**Alfredo Santana**

**Diana Prieto-Santa**

Department of Industrial and Management Systems Engineering

University of South Florida, Tampa, FL 33620

Email: alexs@usf.edu

March 10, 2010

## **Abstract**

Pandemic outbreaks can entail an enormous loss of human life amplified by staggering economic ramifications. At the same time, as pointed out by a number of national academies, decision support methodologies for developing dynamic mitigation strategies have been largely unavailable. In this paper, we present a large-scale simulation-based optimization methodology for developing dynamic predictive mitigation strategies for a network of regional pandemic outbreaks. The methodology incorporates varying virus epidemiology and population dynamics, and generates a progressive allocation of a limited resource budget, including stockpiles of vaccines and antiviral, healthcare capacities for vaccination and antiviral therapy, and social distancing enforcement resources. The optimization control seeks to dynamically minimize the impact of ongoing outbreaks and the expected impact of potential outbreaks. The methodology considers measures of morbidity, mortality, and social distancing, translated into the societal and economic costs of lost productivity and medical expenses. The model was calibrated using historic pandemic data and implemented on a sample cross-regional outbreak in Florida, U.S., with over four million inhabitants. We present a sensitivity analysis for estimating the marginal impact of changes in the total budget availability and variability of some critical factors, including vaccine and antiviral efficacy, and social distancing declaration threshold, duration, and target population conformance. We also analyze the affect of social distancing policies on the dynamics of societal and economic costs. The analysis is done for low and high transmissibility scenarios. The methodology is intended to assist public health policy makers in developing effective mitigation strategies for large-scale cross-regional pandemic outbreaks.

**Keywords:** pandemic influenza, mitigation strategy, dynamic, predictive, vaccination, antiviral, social distancing.

# 1 Introduction and Motivation

Pandemic influenza (PI) outbreaks have historically entailed enormous societal calamities aggravated by tremendous economic forfeitures. The Spanish flu outbreak of 1918-1919, attributed to avian virus serotype H1N1, was exceptionally severe with the case fatality ratio higher than with any other pandemic to date. An estimated 500 million people were infected, worldwide, with the death toll ranging between 40 and 100 million [1]. In large U.S. cities, more than 10,000 deaths per week were reported during the sixteen week period the pandemic raged. By its end, nearly 50% of the U.S. population was infected, and approximately 1% died. In contrast, during regular annual influenza outbreaks, between 10 and 20% of the population is infected, with a 0.008% mortality. Two subsequent outbreaks, the Asian flu (1957, H2N2) and the Hong Kong flu (1968, H3N2), resulted in more than 70,000 and 34,000 deaths, respectively, in the U.S. alone [2]. Nowadays, most experts have an ominous expectation that the next pandemic will likely be caused by an emerging highly pathogenic virus subtype, to which there is little or no preexisting immunity in humans [1].

Since 2003, a series of scattered local outbreaks of the avian-to-human transmittable H5N1 virus has been mapping its way with increased periodicity through Asia, the Pacific region, Africa, Europe, and the Near East [3]. As of December 2009, the World Health Organization (WHO) has reported 447 confirmed infected cases which resulted in 263 mortalities, worldwide [4]. Although instances of H5N1 *human-to-human* transmission have rarely shown up in the recent statistics, ever-mutating emerging virus strains with unpredictable epidemiology pose a menacing threat to the global society. A milder human-to-human transmissible H1N1 virus subtype resurfaced in Mexico in the Spring of 2009 and swiftly propagated to an ongoing global H1N1 pandemic outbreak. As of late December 2009, 208 countries have been affected with a total number of mortalities of at least 11,516 [5].

Combating influenza pandemic outbreaks and effectively addressing natural and societal problems entailing such scourges have to invariably rely on understanding of near real-time evolution of virus epidemiology and population dynamics. The practicality and effectiveness of mitigation strategies also heavily depend on available emergency response infrastructure, mitigation resources, and allocation policies. At present, although the most commonly studied virus strain H5N1 has reached a worldwide case fatality ratio of more than 60% in recent years [4], prediction of the exact emerging virus subtype remains a challenging task. With a modern technology, even after a new virus subtype is identified, a surge production of adequate stockpiles of a potent vaccine can take up to six months [6, 7]. This may prove to be forbiddingly long for the vaccine to be an effective containment measure in the critical onset stage of the pandemic. In the best case scenario, even if the emerged subtype has a known epidemiology, the existing stockpiles would be insufficient [8, 9]. Furthermore, supply of antiviral drugs, immunizers and other healthcare providers, hospital beds, social distancing conformance resources, and logistics will also be substantially constrained. Hence, development of mitigation strategies must be done amidst limited knowledge of disease and population dynamics, constrained infrastructure, limited availability and effectiveness of clinical treatments, and to-be-proven resource allocation policies. This challenge, attested by the recent H1N1 outbreak, has been acknowledged by WHO [9] and echoed by national public health authorities, including the U.S. Centers for Disease Control and Prevention (CDC) and the Department of Health and Human Services (HHS) [10, 11].

## 2 Status of Current Literature

The existing general literature on pandemic modeling aims to address various aspects of the pandemic process including (i) underlying spatio-temporal structure, (ii) contact mechanism, (iii) disease transmission, (iv) disease natural history, and (v) development of containment and mitigation strategies. These aspects are closely interrelated. For instance, the nature of the spatio-temporal structure, including composition of the social mixing groups and temporal dynamics of the affected population, drives the contact process which is the main determinant of the disease transmission [12, 13, 14, 15]. A comprehensive decision-aid model for containment and mitigation must take into account all of the above constituents; it must incorporate the mechanism of disease progression, from initial infection, to asymptomatic earlier phase, symptom manifestation, and final health outcome (recovery or death) [16, 17, 18]; it must also consider the population dynamics of disease spread, including individual susceptibility [19, 20], transmissibility [16, 21, 22, 23], and human behaviors that mediate infection generation [24, 25, 26, 27]; finally, it must incorporate the impact of pharmaceutical and non-pharmaceutical prevention and intervention, including vaccination, antiviral therapy, social distancing, school and workplace closures, travel restrictions, and use of low-cost measures, such as face masks and hand washing [2, 15, 18, 28, 29, 30, 31, 32, 33]. In essence, effective mitigation strategies have a two-fold objective: (i) to systemically alter the disease dynamics and control disease progression with available clinical therapies, and (ii) to intervene the social dynamics and contain disease propagation within the affected communities. Mitigation strategies vary in the composition of the target groups, geo-spatial coverage, and implementation time.

The current literature on assessment and development of PI containment and mitigation strategies can be broadly classified into (i) statistical models, (ii) mathematical models, (iii) simulation-based approaches, and (iv) combinations of thereof. In what follows, we present a summary survey of these approaches, mostly focusing on the simulation-based approaches.

*The statistical models*, driven mainly by likelihood or regression-based approaches, have primarily been used for epidemiological parameter assessment and estimation of the pandemic impact [23, 34, 35]. Traditionally, these models have inherently featured relatively simple and general spatio-temporal structures (e.g., homogeneous social mixing groups [22, 36, 37, 38]).

*The mathematical models* have mostly focused on modeling virus spread and policy assessment [12, 24, 39, 40, 41, 42]. Notable examples of such models are dynamic compartmental approaches, typically represented in the form of a set of differential equations, which delineate transitions between disease phases (e.g., susceptible, exposed, symptomatic infected, etc.). Based on the solution approach, the mathematical models can be subdivided into analytical (or closed form) and iterative. Compared to the statistical approaches, the dynamic-iterative models feature more granular composition of the mixing groups [12, 33]. However, the degree of granularity is still limited since any additional spatio-temporal considerations can negatively impact the computational robustness of the models. Description of the contact processes in most of these models is also somewhat generic and does not take into account changes in the behavioral patterns (e.g., compliance to intervention, such as vaccination and social distancing) during the course of the pandemic. Furthermore, these models are generally based on the infection pathways and disease progression that are invariant to time and individual attributes.

*Simulation-based approaches* have been used for modeling virus spread and assessment and generation of pharmaceutical and/or non-pharmaceutical interventions [2, 14, 15, 31, 43, 44, 45, 46, 47]. Based on the way of generating disease progression, these models can be categorized as agent-based (which track infection pathway of each individual entity) or event-based (which are driven by occurrence of infection events). In contrast to the statistical and mathematical models, agent-based simulations are capable of providing most detailed description of population dynamics whereby each agent is assigned a set of individual attributes (e.g., age, gender, community, etc), that can be modified without altering the general model structure. However, such comprehensive descriptive granularity is achieved at the expense of higher data demand and substantial computational burden. As the result, most existing simulation-based approaches incorporate statistical and/or mathematical submodels (e.g., infection generation) in order to attain an effective balance between model accuracy and practicality.

In recent years, the simulation-based models have focused on integration of therapeutical and non-therapeutical prevention and intervention, to develop synergistic strategies aimed at result-oriented use of constrained resources. These approaches first aim to implement a form of social distancing to reduce the contact between the susceptible and the infected. The infected population is then treated with an antiviral therapy to lessen infectiousness, and the susceptible are vaccinated to elevate their immunity. For example, [15] implemented social distancing for all contacted and symptomatic cases followed by antiviral application. Such strategies, which appear to be more discriminating and thus less expensive, have been found to be particularly efficient for low transmissibility scenarios (i.e., scenarios with the values of the basic reproduction number below 1.8 [44, 48]).

Most notable among recent efforts is a 2006-2007 initiative by MIDAS, the Models of Disease Infectious Agent Study network, which studied three independent simulation models [49]. These models were used to emulate large-scale PI spread for rural areas of Asia [44, 50], U.S. and U.K. [14, 45], and the city of Chicago [51]. MIDAS cross-validated the models by simulating the city of Chicago, with 8.6M inhabitants, and implementing targeted layered containment (TLC). Under TLC, the symptomatic infectious cases refrain from going to work (take liberal leave), receive antiviral treatment, and become subject to household quarantine; the asymptomatic contacts receive targeted antiviral prophylaxis (TAP) and become subject to household quarantine. The research findings of the MIDAS network and other institutions [18, 31] were used in a recent “Modeling Community Containment for Pandemic Influenza” report by the Institute of Medicine (IOM), U.S., to formulate a set of recommendations for mitigating PI at the local level [52]. These recommendations were used in a pandemic preparedness guidance developed jointly by CDC, HHS, and other federal U.S. agencies [53].

**The IOM report [52] points out several limitations of the MIDAS models**, observing that “*because of the significant constraints placed on the models*” being considered by policy makers, “*the scope of models should be expanded.*” The IOM recommends that “*steps be taken now to adapt or develop decision-aid models that can be readily linked to surveillance data to provide real-time feedback during an epidemic. Research protocols should be developed, approved, and put in place now to generate the information needed during an outbreak to inform models, and improve their disease sub-models.*” The report also strongly recommends 1) “*that future modeling efforts incorporate broader outcome measures ... to include the costs and benefits of intervention strategies*”, and 2) “*that models examining*

*the potential effectiveness of school and workplace closures on mitigating pandemic influenza include a broader range of closure options.”* We add here that most current approaches focus on assessment of policies defined *a priori*; few of the existing models for design of synergistic mitigation strategies are “*learning*”, i.e., capable of predicting of and adapting to changes in the course of a pandemic, and ultimately generating a dynamic optimal strategy [47]. Furthermore, the majority of the current simulation models feature a single-region design (see Appendix, Table 1). In [47], we developed a simulation-based optimization model for generating mitigation strategies for cross-regional pandemic outbreaks. The model was implemented on a sample outbreak and the resultant strategy was compared to the existing governmental pro-rata distribution policy, which allocates mitigation resources to each affected region in proportion to its population [54].

In this paper, we present a novel decision-aid methodology for developing dynamic predictive mitigation strategies for a network of regional pandemic outbreaks. The methodology is driven by a large-scale simulation-based dynamic optimization model that incorporates varying virus epidemiology and region-specific population dynamics. The model generates mitigation strategies for an efficient, progressive allocation of limited resources, including stockpiles of vaccines and antiviral drugs, healthcare capacities for administration of vaccination and antiviral therapy, and social distancing enforcement resources. The optimization control seeks to dynamically minimize the impact of ongoing outbreaks and the expected impact of potential outbreaks, and allocates the resources accordingly. The methodology considers measures of morbidity, mortality, and social distancing, translated into the cost of lost productivity and medical expenses (societal and economic costs). The model was calibrated using historic pandemic data and tested on a sample cross-regional outbreak in Florida, U.S., with over four million inhabitants. We also present a sensitivity analysis for estimating the marginal impact (measured in terms of the average total pandemic cost and the average number of fatalities) of changes in the total budget availability and variability of some critical decision factors. These factors included: (i) vaccine efficacy, (ii) efficacy of antiviral therapy, (iii) social distancing conformance level, (iv) social distancing declaration threshold, and (v) social distancing period.

Compared to our previous work in [47], this paper features the following main advances: (i) in [47], progressive resource allocations are irrevocable, i.e., once resources are allocated to an affected region, they remain in the region until full depletion, regardless of the posterior dynamics of the overall pandemic; in contrast, our model is capable of re-allocating the resources remaining from the previous distributions, based on the current pandemic status, and thus achieving a more efficient resource utilization; (ii) our model incorporates the cost of the resources (e.g., vaccines, antiviral, etc.) and strives to allocate a total available budget, as opposed to a separate allocation of total available quantities of individual resources, which vary significantly in their relative cost and effectiveness; (iii) our model investigates optimal policy generation under two scenarios of virus severity: low transmissibility and high transmissibility, as opposed to a high transmissibility analysis in [47]; (iv) our study attempts to analyze the affect of social distancing policies (namely, the target population conformance) on the dynamics of societal and economic costs; (v) in this paper, we also present a short description of our decision-aid simulation software made freely available to general public through our website.

This paper has the following organization. In Section 3, we present our simulation-based opti-

mization methodology, including description of the population dynamics and disease transmission, the mechanism of disease progression, and therapeutical and non-therapeutical intervention, followed by description of the calibration methodology for single-region and cross-regional simulation models, and presentation of the optimization control model. In Section 4, results of the testbed implementation are presented, followed by discussion of the sensitivity analysis. Conclusions are given in Section 5.

### 3 Simulation-Based Optimization Model

Our large-scale simulation-based optimization model generates predictive strategies to allocate a total available budget of mitigation resources over a network of regional pandemic outbreaks, progressively, from one affected region to the next. Mitigation resources include stockpiles of vaccine(s) and antiviral drug(s), hospital beds, capacities for vaccination and antiviral administration, social distancing enforcement resources, among others. The methodology subsumes a cross-regional simulation model, a set of single-region simulation models, and an overarching dynamic optimization control.

The regions inside the network are classified as unaffected, ongoing outbreak (which includes new outbreak), and contained (see Fig. 1). The regions are interconnected by air and land travel, which is emulated by the cross-regional model. The single-region model mimics the population and disease dynamics inside each ongoing region, impacted by available pharmaceutical and non-pharmaceutical prevention and intervention. The pandemic spreads from ongoing to unaffected regions by infectious travelers who pass through regional border control. At every new regional outbreak epoch, the cross-regional model invokes the optimization control, which allocates the total available resource budget, including remaining resources from the previous allocations, to the new/ongoing outbreak regions (*actual allocation*)

and potential (unaffected) outbreak regions (*virtual allocation*). The objective function of the optimization model incorporates measures of morbidity, mortality, and social distancing, translated into the cost of lost productivity and medical expenses. The objective function strives to minimize the cost of the new/ongoing outbreaks and the expected cost of the potential outbreaks, spreading from the ongoing regions. Detailed daily pandemic statistics is collected for each affected region, including the numbers of new infected, deceased, and quarantined cases, for different age groups. As the regional outbreaks become contained, the model estimates their actual societal and economic costs.

In the remainder of this section, we present the details of the cross-regional simulation model (Section 3.1) and the single-region simulation model (Section 3.2), including the description of the calibration methodology (Section 3.3). The dynamic optimization control model is presented in Section 3.4,

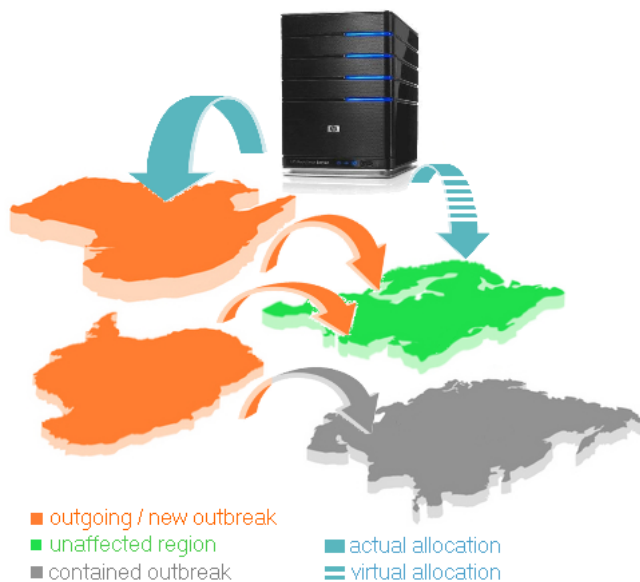


Figure 1: Schematic of simulation-based optimization methodology

followed by analysis of the results of the testbed implementation in Section 4.

### 3.1 Cross-Regional Simulation Model

The cross-regional simulation model emulates propagation of pandemic across the network of affected regions. It controls a set of single-region simulation models of ongoing outbreaks and invokes the optimization model for actual and virtual resource allocation at every new outbreak epochs. The schematic of the cross-regional simulation model is presented in Fig. 2.

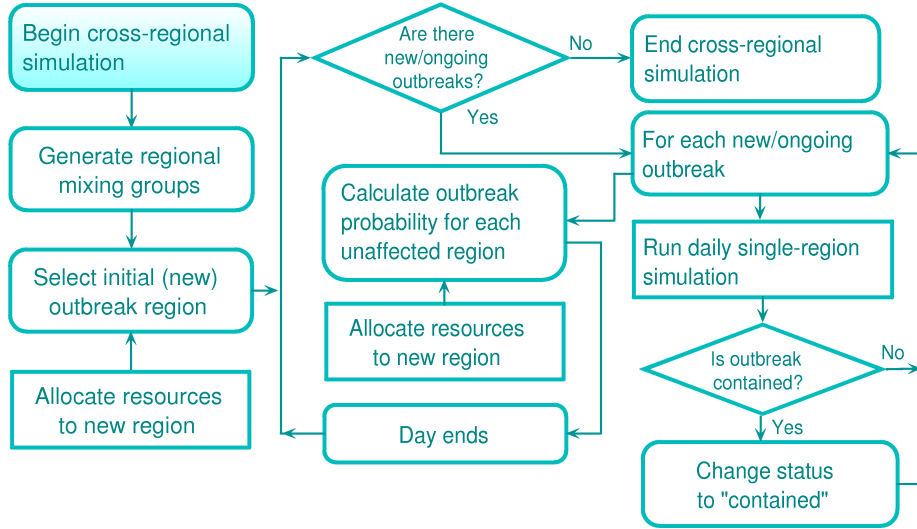


Figure 2: Schematic of cross-regional simulation model

The model is initialized by generating mixing groups and population dynamics for each network region (for details, see Section 3.2.1). A pandemic is triggered by injecting one or more infectious cases into a randomly selected region, designated as the initial outbreak region. Details associated with the resulting contact dynamics and disease propagation within the region are presented in Section 3.2. As the symptomatic cases start seeking medical assistance, the new regional outbreak is detected. At this point, the model calls the optimization control which generates a resource allocation (see Section 3.4). The cross-regional simulation then passes control back to the single-region model, which executes a cycle (e.g., daily) of the regional disease and population dynamics, now mediated by the allocated clinical therapies and social distancing measures (see Section 3.2). The simulation clock inside the single-region routine advances in smaller time increments (e.g., hourly; see Section 4).

As the outbreak intensifies, it spreads over to the unaffected regions, as infectious travelers pass undetected through air and land border control with some probability (the probabilities are different for asymptomatic and symptomatic cases). Travelers are considered to act independently. Each infectious traveler is assumed to initiate a regional outbreak with an equal, time-homogeneous probability  $\omega$  for the entirety of his/her infection period, regardless of his/her point of origin. For each unaffected region, the outbreak probability at time  $t > 0$ ,  $P_t$ , is calculated using the binomial probability law, as follows

$$P_t = 1 - (1 - \omega)^{n_t}, \quad (1)$$

where  $n_t$  denotes the number of infectious travelers in the region at time  $t$ . Based on the outbreak

probability value, the cross-regional model determines which of the unaffected regions have become new outbreaks (in the testbed implementation, the values of  $P_t$  were computed once at the end of each day). The model also determines if an outbreak has been contained, based on a certain threshold of the daily infection rate. The cross-regional simulation ends when all outbreaks have been contained.

### 3.2 Single-Region Simulation Model

The single-region simulation model emulates population and disease dynamics within an affected region.

A schematic of the model is shown in Fig. 3. The model subsumes the following main components: (i) population dynamics, (ii) contact and infection process, (iii) disease natural history, and (iv) mitigation prevention and intervention, including measures of social distancing, vaccination, and antiviral application. The model collects detailed regional influenza statistics, including numbers of infected, recovered, deceased, and quarantined cases, for different age

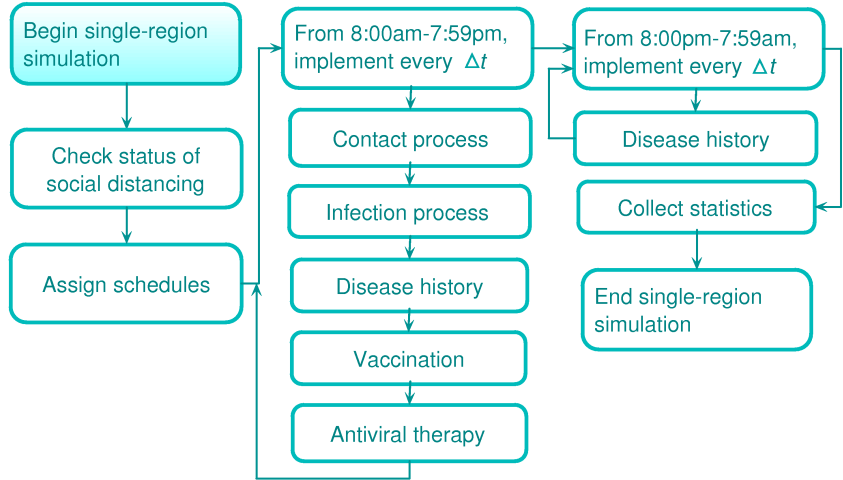


Figure 3: Schematic of single-region simulation model

groups. For a contained outbreak, its societal and economic costs are calculated. The societal cost includes the cost of lost lifetime productivity of the deceased; the economic cost includes the cost of medical expenses of the recovered and deceased and the cost of lost productivity of the quarantined (see Section 4.1.3). The single-region simulation model builds upon a prototype presented in [43].

At any point of time, the population of an ongoing region is assumed to be composed of the following exclusive compartments: susceptible, contacted, infected, recovered, and deceased (see Fig. 4).

During the course of his/her social interaction, a susceptible individual may periodically come into contact with infectious cases. The contacted individual then either becomes infected with a certain probability  $p$  or returns to the compartment of susceptibles. An infected case then either dies with a certain probability  $m$  or recovers. It is further assumed that a recovered person develops immunity and cannot be susceptible again. All recovered cases continue circulating through the mixing groups. In what follows, we present the details of our modeling approach for the fundamental components of the single-region simulation model.

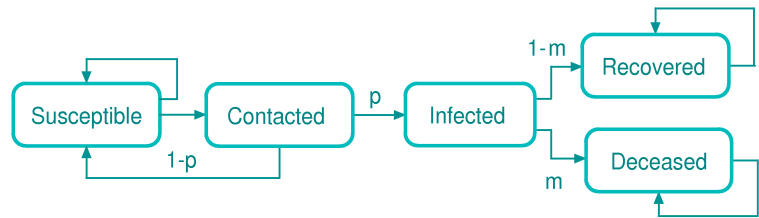


Figure 4: Schematic of the disease progression model

### 3.2.1 Population Dynamics

We model a region as a set of population centers composed of *mixing groups* of various types, including households, offices, manufacturing facilities, universities, schools, churches, shopping centers, entertainment centers, etc. A household consists of household members, each of which is assigned a comprehensive set of attributes including age, gender, parenthood, workplace, immunity status, infection susceptibility, probability of travel, and others. Each inhabitant is also assigned  $\Delta t$  time-discrete (e.g.,  $\Delta t = 1$  hour) weekday and weekend schedules, which depend on a number of factors, including: (i) age and parenthood, (ii) inhabitant’s disease status, (iii) travel status, (iv) social distancing decrees in place, and (v) inhabitant’s conformance to them. As their schedules advance, inhabitants circulate throughout the mixing groups, staying a certain amount of time in each of them.

### 3.2.2 Contact and Infection Processes

Disease transmission occurs through contact events between infectious and susceptible individuals within the mixing groups. At the beginning of every  $\Delta t$  units of time (e.g., one hour), for each mixing group  $g$ , the simulation model tracks the total number of infectious cases  $n_g$  present in the group. Each infectious case randomly generates  $r_g$  per  $\Delta t$  unit of time *new contacts*, uniformly, from the susceptible cases present in the mixing group. We assume the following simplifying characterization of the contact process: (i) during  $\Delta t$  period, a susceptible may come into contact with at most one infectious case and (ii) each contact exposure lasts  $\Delta t$  units of time. Once a susceptible has started a contact exposure at time  $t$ , he/she will develop into an infectious case at time  $t + \Delta t$  with a certain probability that is calculated as shown below.

Let  $L_i(t)$  be a nonnegative continuous random variable that represents the duration of contact exposure, starting at time  $t$ , that is required for a contact  $i$  to become infected. We assume that  $L_i(t)$  follows an exponential distribution with parameter  $\lambda_i(t)$ , where  $\lambda_i(t)$  represents the instantaneous force of infection applied to contact  $i$  at time  $t$  [39, 55, 56]. The probability that a susceptible  $i$ , whose contact exposure has started at time  $t$ , will develop into an infectious case at time  $t + \Delta t$  is then given as

$$P\{L_i(t) \leq \Delta t\} = 1 - e^{-\lambda_i(t)\Delta t}. \quad (2)$$

### 3.2.3 Disease Natural History

It is assumed that upon becoming infected, an individual enters simultaneously into the phases of latency and incubation (see Figure 5). During the incubation phase, the individual stays asymptomatic (i.e., shows no visible symptoms). At the end of the latency phase, the individual becomes infectious and enters the infectious phase [45, 49, 50, 57]. At the end of the incubation period, the individual becomes symptomatic. At the conclusion of the infectious period, the individual enters the final disease stage which culminates in his/her recovery or death.

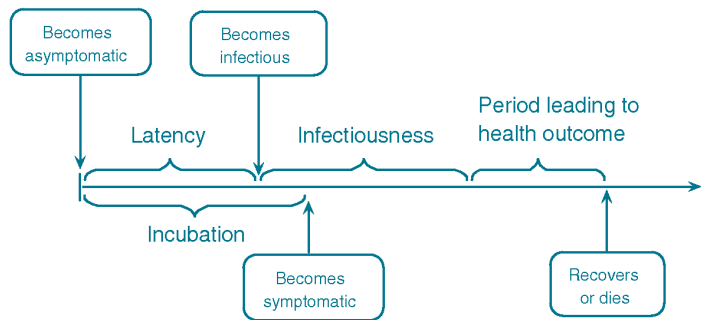


Figure 5: Schematic of disease natural history model

Mortality for influenza like diseases is a complex process, which is affected by a number of factors and variables. For most of these variables, little or no accurate data has been collected from past pandemics. In addition, the time of death could oftentimes be weeks following the disease episode (mainly attributable to subsequent pneumonia related complications [58]). Because of the uncertainty underlying the mortality process, we adopted a simplified, age-based form of the mortality probabilities, where the mortality probability of infected  $i$ ,  $m_i$  is given as

$$m_i = \mu_i - \tau \rho_i, \quad (3)$$

where  $\mu_i$  is the age-dependent base mortality probability of infected  $i$ ,  $\rho_i$  is his/her status of antiviral treatment (0 or 1), and  $\tau$  is the efficacy of the antiviral therapy, measured in terms of the reduction in the base mortality probability [50].

### 3.2.4 Mitigation Prevention and Intervention

Mitigation prevention and intervention considered in the single-region model include pharmaceutical and non-pharmaceutical measures. Implementation of the mitigation measures is initiated upon detection of the first confirmed infected case [59]. At this point, mitigation resources are assigned (see Section 3.4) and deployed in the region. The model considers a certain outbreak detection delay and a delay for deployment of field responders.

*Pharmaceutical mitigation.* Pharmaceutical prevention and intervention consist of vaccination and antiviral application. Vaccines are offered to the individuals from a prespecified risk group, to reduce their infection susceptibility. It is assumed that a certain fraction of the risk group will not comply with vaccination. Once administered, the vaccine takes a certain period to become effective (typically, between 10 and 14 days) [60]. Vaccination is constrained by the available stockpile and the administration capacity, measured in terms of the number of immunizer-hours.

For antiviral application, we assume that a certain fraction of symptomatic infected cases will seek medical assistance [61, 62]. Those of them who belong to a prespecified mortality risk group, receive an antiviral treatment, to reduce their mortality probability (see Eq. 3). It is assumed that an antiviral becomes effective immediately. The antiviral application is subject to availability of the antiviral stockpile and the administration capacity, measured in terms of the number of certified nurses. Both the antiviral application and vaccination are affected by a number of social behavioral factors, including conformance of the target population, its degree of risk perception, and associated compliance of healthcare personnel [63, 64, 65]. The conformance level of the target population could be affected by the demographical profile of the region [66, 67, 68, 69, 70] and quality of the public information available [71], among other factors. The degree of risk perception of the target population could be impacted by a negative experience developed during pharmaceutical campaigns of the previous outbreaks [72, 73], as well as by public fear and rumors [74, 75].

*Non-pharmaceutical mitigation.* For a social distancing mediation, we adopted a guidance suggested by CDC, U.S. [53]. The guidance establishes five categories of pandemic severity (from 1 to 5) and recommends different quarantine and closure policies for each of the categories. The categories are determined based on the value of the case fatality ratio (CFR), the cumulative proportion of the

number of fatalities in the total infected population. Our simulation model periodically reassesses the CFR value during the pandemic course. For the CFR values lower than 0.1% (which corresponds to Category 1), voluntary at-home isolation of the infected cases is *implemented*. If the CFR falls in the range between 0.1% and 1.0% (Categories 2 and 3), in addition to the above at-home isolation, the following measures are *recommended*: (i) voluntary quarantine of households members of infected cases and (ii) child and adult social distancing. Finally, for the CFR values exceeding 1.0% (Categories 4 and 5), all the above measures are *implemented*. Alike pharmaceutical measures, the effectiveness of social distancing mitigation is also affected by several of the behavioral factors mentioned above [71]. Our model considers a certain social distancing conformance level, which can vary based on the demographics profile. Travel restrictions considered in the model included regional air and land border control for outgoing infected travelers (for details, see the testbed implementation in Section 4).

### 3.3 Calibration Methodology for the Single-Region Model

The single-region simulation model was calibrated using two commonly accepted measures of pandemic severity: the *basic reproduction number* ( $R_0$ ) and the *infection attack rate* ( $IAR$ ).  $R_0$  is defined as the average number of secondary infections, produced by a typical infected case in a totally susceptible population. Our model with its a detailed, person-to-person infection generation traceability allows identification of all secondary infections created by each infected case. All infected cases are then classified by generation of infection, as in [31, 44], where a generation is defined as the set of all infected cases (offsprings) that are at the same tier of descent from their infection generators (ancestors) [56]. The value of  $R_0$  is then calculated as the average reproduction number of a typical generation in the early stage of the pandemic when no interventions are implemented (known as the *baseline* scenario). Our model was calibrated to attain the baseline values of  $R_0$  similar to those obtained from historic pandemic data [44, 48] (see Section 4.1.2).

$IAR$  is defined as the ratio of the total number of infections over the pandemic period to the size of the initial susceptible population. To further calibrate our model, we used the following relationship between baseline  $R_0$  and  $IAR$ , as presented in [15, 56]:

$$R_0 = \frac{-\ln(1 - IAR)}{IAR}, \quad \text{for } R_0 \geq 1, 0 < IAR < 1. \quad (4)$$

Section 4.1.2 of this paper provides the details of the calibration process for a sample testbed scenario.

### 3.4 Decision Support Optimization Model

The optimization model is invoked at every new outbreak epoch to allocate the total available resource budget, including remaining resources from the previous allocations, to the new/ongoing outbreak regions (*actual allocation*) and potential outbreak regions (*virtual allocation*). By doing so, the model seeks to progressively minimize the impact of ongoing outbreaks and the expected impact of potential outbreaks. Mitigation resources include stockpiles of vaccine(s) and antiviral drug(s), hospital beds, capacities for vaccination and antiviral administration, social distancing enforcement resources, among others. The objective function of the optimization model incorporates measures of morbidity, mortality,

and social distancing, translated into the cost of lost productivity and medical expenses. In what follows, we present the details of the model. We introduce the following notation.

$S$  = the set of all regions,

$A^n$  = the set of regions in which pandemic is contained at the  $n^{\text{th}}$  outbreak epoch ( $n = 1, 2, \dots$ ),

$B^n$  = the set of ongoing regions at the  $n^{\text{th}}$  outbreak epoch,

$C^n$  = the set of unaffected regions at the  $n^{\text{th}}$  outbreak epoch,

$M^n$  = budget availability at the  $n^{\text{th}}$  outbreak epoch,

$R$  = the set of available types of mitigation resources ( $R = \{1, 2, \dots, r\}$ ),

$c_i$  = unit cost of type  $i$  resource,  $i \in R$ ,

$\hat{q}_i^n$  = amount of resource  $i$  remaining from previous allocations, at the  $n^{\text{th}}$  outbreak epoch.

Let  $TC_k^n$  denotes the total cost of an outbreak in region  $k$  at the  $n^{\text{th}}$  outbreak epoch. The total cost is a function of the *decision variables*  $q_{ik}$  which denote the amount of resource  $i$  allocated to region  $k$ . We assume that outbreaks occur one at a time. At the  $n^{\text{th}}$  new outbreak epoch in region  $j$ , the following optimization problem is invoked

$$\text{Min } TC_j^n(q_{1j}, q_{2j}, \dots, q_{rj}) + \sum_{l \in B^n \setminus \{j\}} TC_l^n(q_{1l}, q_{2l}, \dots, q_{rl}) + \sum_{s \in C^n} TC_s^n(q_{1s}, q_{2s}, \dots, q_{rs}) \cdot p_s^n$$

subject to

$$\sum_{i \in R} c_i \cdot q_{ij} + \sum_{l \in B^n \setminus \{j\}} \sum_{i \in R} c_i \cdot q_{il} + \sum_{s \in C^n} \sum_{i \in R} c_i \cdot q_{is} \cdot p_s^n - \sum_{i \in R} c_i \cdot \hat{q}_i^n \leq M^n$$

$$q_{ij} + \sum_{l \in B^n \setminus \{j\}} q_{il} + \sum_{s \in C^n} q_{is} \cdot p_s^n \geq \hat{q}_i^n, \quad \forall i \in R.$$

In the above objective function, the first term represents the total cost of the new outbreak  $j$ , estimated at the  $n^{\text{th}}$  outbreak epoch, and based on the actual resource allocation  $\{q_{1j}, q_{2j}, \dots, q_{rj}\}$ . The second term represents the total cost of ongoing outbreaks, excluding region  $j$ , which is (re)estimated at the  $n^{\text{th}}$  outbreak epoch, based on the current pandemic status (for details, see below). This cost is a function of the allocation  $\{q_{1l}, q_{2l}, \dots, q_{rl}\}$ , which may include amounts remaining from previous allocations. The third term represents the total expected cost of outbreaks in currently unaffected regions, based on the virtual allocation  $(q_{1s}, q_{2s}, \dots, q_{rs})$  and the regional outbreak probabilities  $p_s^n$ .

The first model constraint relates the total available budget with the value of the current actual and virtual resource allocations, adjusted with the value of the resources remaining from the previous allocations. The second set of constraints guarantee that the needs of the current actual and virtual allocations will first be satisfied using the resources remaining from the previous allocations (the outstanding resource needs will then be fulfilled from the remaining budget).

The total cost of an outbreak in region  $k$  at the  $n^{\text{th}}$  outbreak epoch is calculated as following

$$TC_k^n = \sum_{h \in \mathcal{H}} (m_h + \bar{w}_h) X_{hk}^n + \sum_{h \in \mathcal{H}} \bar{w}_h \cdot Y_{hk}^n + \sum_{h \in \mathcal{H}} \hat{w}_h \cdot D_{hk}^n + \sum_{h \in \mathcal{H}} w_h \cdot V_{hk}^n,$$

where

$\mathcal{H}$  = the set of age groups,

$m_h$  = total medical cost of an infected case in age group  $h$  over his/her disease period,

$\bar{w}_h$  = total cost of lost wages of an infected case in age group  $h$  over his/her disease period,  
 $\hat{w}_h$  = cost of lost lifetime wages of a deceased case in age group  $h$ ,  
 $w_h$  = daily cost of lost wages of a non-infected case in age group  $h$  who complies with quarantine,  
 $X_{hk}^n$  = total number of infected cases in age group  $h$  who seek medical assistance,  
 $Y_{hk}^n$  = total number of infected cases in age group  $h$  who do not seek medical assistance,  
 $D_{hk}^n$  = total number of deceased cases in age group  $h$ ,  
 $V_{hk}^n$  = total number of person-days of cases in age group  $h$  who comply with quarantine.

Variables  $X_{hk}^n$ ,  $Y_{hk}^n$ ,  $D_{hk}^n$ , and  $V_{hk}^n$  are defined for region  $k$  at the  $n^{\text{th}}$  outbreak epoch. We determine the value of  $X_{hk}^n$  using the following regression model

$$X_{hk}^n = \delta_{hk}^0 + \sum_{i \in R} \delta_{hk}^i \cdot q_{ik} + \sum_{i, m \in R, i \neq m} \delta_{hk}^{im} \cdot q_{ik} \cdot q_{mk}, \quad (5)$$

where  $\delta_{hk}^i$  denotes the regression coefficient associated with resource  $i$ , and  $\delta_{hk}^{im}$  is the regression coefficient for the interaction between resources  $i$  and  $m$ . Similar expressions are used for  $Y_{hk}$ ,  $D_{hk}$ , and  $V_{hk}$ .

We have that  $p_k^n = \sum_{l \in B^n} p_{lk}^n$ , where  $p_{lk}^n$  denotes the outbreak probability in region  $k$ , caused by an ongoing outbreak in region  $l$ , estimated at the  $n^{\text{th}}$  outbreak epoch. This probability is considered to be a function of the resource allocation for region  $l$  at the  $n^{\text{th}}$  outbreak epoch, and is calculated using the following regression model

$$p_{lk}^n = \gamma_{lk}^0 + \sum_{i \in R} \gamma_{lk}^i \cdot q_{il} + \sum_{\substack{i, m \in R \\ i \neq m}} \gamma_{lk}^{im} \cdot q_{il} \cdot q_{ml},$$

where  $\gamma_{lk}^i$  denotes the regression coefficient associated with resource  $i$ ,  $\gamma_{lk}^{im}$  is the regression coefficient associated with interaction between resources  $i$  and  $m$ , and  $\gamma_{lk}^0$  represents the intercept.

### 3.5 Solution Algorithm

Below we present the solution algorithm for the simulation-based optimization model.

1. Estimate regression equations for all regions using the single-region simulation model.
2. Set  $n = 1$ . Initialize sets of regions:  $A^n = \emptyset$ ,  $B^n = \emptyset$ ,  $C^n = S$ .
3. Select randomly the initial outbreak region  $j$ .
4. Update sets of regions:  $B^n \leftarrow B^n \cup \{j\}$  and  $C^n \leftarrow C^n \setminus \{j\}$ .
5. Solve the resource allocation model for region  $j$ . Update the total budget availability.
6. If  $B^n \neq \emptyset$ , do Step 7. Else, do Step 9.
7. (a) For each ongoing region, implement a next day run of its single-region simulation.  
(b) Check the containment status of each ongoing region. Update sets  $A^n$  and  $B^n$ , if needed.  
(c) For each unaffected region, calculate its outbreak probability.  
(d) Based on the outbreak probability values, determine if there is a new outbreak region(s)  $j$ .  
If there is no new outbreak(s), go to Step 6. Otherwise, go to Step 8.

8. For each new outbreak region  $j$ ,
  - (a) Increment  $n \leftarrow n + 1$ .
  - (b) Update sets  $B^n \leftarrow B^n \cup \{j\}$  and  $C^n \leftarrow C^n \setminus \{j\}$ .
  - (c) Re-estimate regression equations for each region  $k \in B^n \cup C^n$  using the single-region simulations, where each simulation is initialized to the current outbreak status in the region.
  - (d) Determine the remaining availability of the previously allocated resources.
  - (e) Solve the resource allocation model for each region  $k \in B^n$ .
  - (f) Update the total budget availability.
9. Calculate the total cost for each contained region and update the overall pandemic cost.

## 4 Testbed Implementation

A sample cross-regional outbreak scenario included a network of four counties in Florida, U.S.: Hillsborough, Miami Dade, Duval, and Leon, with populations of 1.0, 2.2, 0.8, and 0.25 million people, respectively. The H5N1 virus subtype was considered. A basic unit of time  $\Delta t$  for people’s schedules, contact dynamics, infection transmission, disease natural history, and implementation of interventions was taken to be one hour (see Fig. 3 and Eq. 2). Each regional simulation was run for a period (up to 185 days) until the number of new daily infections approached near zero (see Section 4.1.3).

### 4.1 Model Parameter Values

This section presents the details on selecting parameter values for cross-regional and single-region models, including parameters of population and disease dynamics, calibration, and mitigation.

#### 4.1.1 Parameters of Population and Disease Dynamics

Demographic and social dynamics data for each of the regions was extracted from the U.S. Census [76] and the National Household Travel Survey [77] (see Appendix, Tables 2-4). Compositions of the regional mixing groups are shown in Appendix, Tables 5-8. In these tables, column 1 and 2 show the mixing group type and the number of mixing groups for each type, respectively. Column 3 shows the probability distribution among the types for assigning the workplaces of inhabitants. Columns 4-6 show the probability distribution among the types for assigning the weekday after-work errands, weekend errands, and errands during quarantine (see also Section 4.1.3), respectively. The last column contains the hourly contact rates for each mixing group type. Daily (hourly) schedules were adopted from [43].

Each infected individual was assigned a daily travel probability of 0.24% [77], of which 7% was by air and 93% by land transportation. The origin-destination travel probabilities within the network of four regions were calculated based on the traffic volume data [78, 79, 80, 81] (see Appendix, Table 9). Infection detection probabilities for regional border controls for symptomatic cases were assumed to be 95% and 90%, for air and land transportation, respectively. These values were reduced by 70% for asymptomatic travelers. Travel bans were implemented for all detected infectious cases. An undetected infectious traveler was assumed to trigger a regional outbreak in his/her destination with a

time-homogeneous probability  $\omega = 0.001$  during his/her infectiousness period. The regional outbreak probabilities  $P_t$  were calculated once at the end of each day using Eq. 1.

The instantaneous force of infection applied to contact  $i$  at time  $t$  ( $\lambda_i(t)$  in Eq. 2) was modeled as

$$\lambda_i(t) = -\ln(1 - p_i(t)), \text{ where } p_i(t) = \alpha_i - \delta\theta_i(t), \quad (6)$$

where  $\alpha_i$  is the age-dependent base instantaneous infection probability of contact  $i$ ,  $\theta_i(t)$  is his/her status of vaccination at time  $t$  (taken as 0 or 1), and  $\delta$  is the vaccine efficacy, measured in terms of the reduction in the base instantaneous infection probability (achieved after 10 days [60]). Note that, as  $p_i(t)$  increases, the instantaneous force of infection  $\lambda_i(t)$  grows at an increasing rate (see Fig. 6). The age-dependent base instantaneous infection probabilities were adopted from [45] (see Appendix, Table 10).

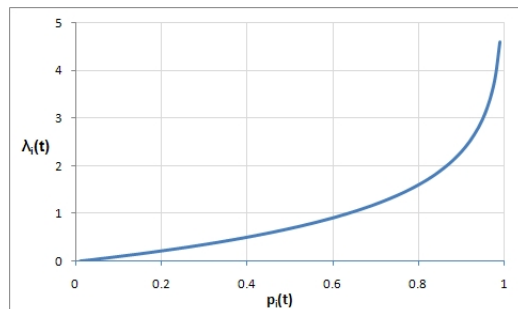


Figure 6:  $\lambda_i(t)$  vs.  $p_i(t)$

The disease natural history for H5N1 virus subtype was taken as the following: a latent period of 29 hours, an incubation period of 46 hours, and an infectiousness period between 29 and 127 hours [82].

The values of the base mortality probability of infected case  $i$ ,  $\mu_i$  (Eq. 3), were determined using the statistics recommended by the Working Group on Pandemic Preparedness and Influenza Response [83]. This data shows the percentage of mortality for age-based high-risk groups (see Appendix, Table 11, columns 1-3). For the testbed scenario, the mortality probabilities for different age groups (Appendix, Table 11, column 4) were estimated using the assumption that high-risk cases are expected to account for 85% of the total number of fatalities, for each age group [83].

#### 4.1.2 Calibration of the Single-Region Models

The single-region simulation models were calibrated against  $R_0$  and  $IAR$  (see Section 3.3), using hourly contact rates within mixing groups. Original contact rates were adopted from [45]. These contact rates were adjusted to obtain the baseline values of  $R_0$  similar to those estimated from past outbreaks [44, 48], for both high and low transmissibility scenarios (see Appendix, Table 12 for a sample of contact rates).

The values of  $R_0$  were estimated for each region using the average reproduction numbers for generations of infection, as presented in [31, 44], over multiple replicates (e.g., see Fig. 7 for the Hillsborough County). As the figure illustrates, generations 5 through 8 (the solid line) and generations 7 to 9 (the dotted line) represent “typical” [31] or representative infectious cases, born in the *early stage* of the pandemic, when most of the regional population is susceptible. For the purpose of computing the value of  $R_0$ , earlier generations were disregarded, as they were composed of a limited number of infected cases with highly variable individual reproduction numbers.

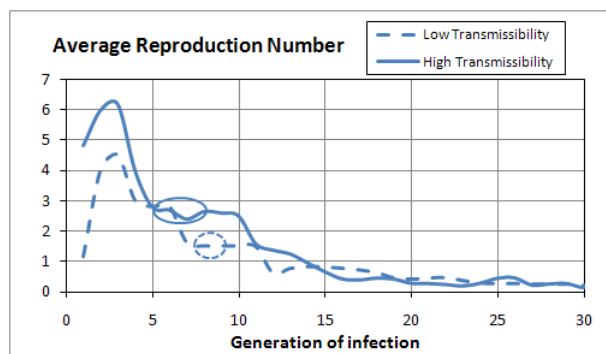


Figure 7: Estimation of  $R_0$  (Hillsborough)

Historically,  $R_0$  values for PI range between 1.4 and 3.9, where PI with  $R_0 \leq 1.8$  are considered as of low transmissibility and PI with  $2.2 \leq R_0 \leq 3.9$  as of high transmissibility [44, 48]. Henceforth, the  $R_0$  value of 2.538 for the high transmissibility testbed (Fig. 7, solid line) and 1.525 for the low transmissibility testbed (Fig. 7, dotted line) were taken, for the Hillsborough County (other regions had similar  $R_0$  values). These values corresponded to the simulated  $IARs$  of 0.881 and 0.538, respectively. Note that from the theoretical relationship in Eq. 4,  $IAR$  of 0.881 and 0.538 yield  $R_0$  of 2.426 and 1.435, respectively. Thus, the simulated  $R_0$  numbers show a good match with the theoretical approximations.

### 4.1.3 Mitigation Related Parameters

The mitigation resources considered in the testbed included stockpiles of vaccines and antiviral, administration capacities for vaccination and antiviral therapy, and quarantine enforcement resources (required to achieve a targeted social distancing conformance level). We assumed a 24-hour CDC resource deployment delay once the first infection case is confirmed [59].

*Pharmaceutical measures.* The vaccination risk group included individuals younger than 5 years and older than 65 years [84]. The risk group for antiviral application included individuals below 15 years and above 55 years [84, 85]. The efficacy levels for the vaccine,  $\delta$  (in Eq. 6) and antiviral,  $\tau$  (in Eq. 3) were assumed to be 40% [50, 86] and 30%, respectively. See Section 4.2.2 for a sensitivity analysis on both parameters. We assumed a 95% target population conformance for both measures. The immunity development period for the vaccine was taken as 10 days [60]; the antiviral was assumed to become effective immediately. Table 13 summarizes vaccination and antiviral treatment resource requirements for each region along with resource costs [87, 88, 89] and the total budget requirement.

*Non-pharmaceutical measures.* A simplified version of the CDC guidance for non-pharmaceutical interventions for Category 5 was implemented (see Section 3.2.4, [53]). Once the case fatality ratio has reached 1.0% in the affected region, a social distancing policy is declared and remains in effect for 14 days [53]. Individuals below a prespecified age  $\xi$  (22 years) were assumed to stay at home during the quarantine period. Of the remaining population, a certain proportion  $\phi$  [90] stayed at home and was allowed a one-hour leave, every three days, to buy essential supplies. The remaining  $(1 - \phi)$  non-compliant proportion followed a regular schedule. All testbed scenarios considered the quarantine conformance level  $\phi$  (a decision variable) bounded between 50% and 80% [71].

An outbreak was considered contained, if the daily new infections did not exceed five cases, for seven consecutive days. Once contained, a region was simulated for an additional 10 days (the natural history period [91]) to allow an accurate estimation of the pandemic statistics. The costs of lost productivity and medical expenses were adopted from [83] and inflation-adjusted using [92] (see Appendix, Table 14).

As presented in Sections 3.4 and 3.5, the optimization model was supported by a set of regression equations, re-estimated at every new outbreak epoch, that related the allocation quantities of mitigation resources with the total number of infections, mortalities, and quarantined cases, for different age groups. For each of the four regions, we developed a  $2^5$  statistical design of experiment, to estimate the regression coefficient values of the significant decision variables (factors) and their interactions. To ease the very significant computational burden, the testbed implementation considered allocation decisions only for new outbreak regions. The simulation code was developed using the C++ language.

Simulations were run on a computer with a Pentium 3.40 GHz processor and 4.0 GB of RAM. The running time for a cross-regional simulation replicate averaged 20 minutes.

## 4.2 Sensitivity Analysis

This section presents a sensitivity analysis for assessing the marginal impact of changes in the total budget availability and variability of some of the critical factors, for both low and high transmissibility scenarios. The marginal impact was measured separately by the change in the total pandemic cost and the number of mortalities (averaged over multiple replicates), resulting from a unit change in the total budget availability or a factor value, one at a time. Factors under consideration included: (i) antiviral efficacy, (ii) vaccine efficacy, (iii) social distancing conformance, (iv) social distancing declaration threshold, and (v) social distancing period. We also investigated the affect of varying the social distancing conformance on the dynamics of the societal and economic costs.

### 4.2.1 Total Budget Availability

Figures 8(a) and 8(b) show the dynamics of the pandemic impact, measured as the average number of fatalities and total cost, for different levels of the total budget availability relative to the total budget requirement (see Appendix, Table 13).

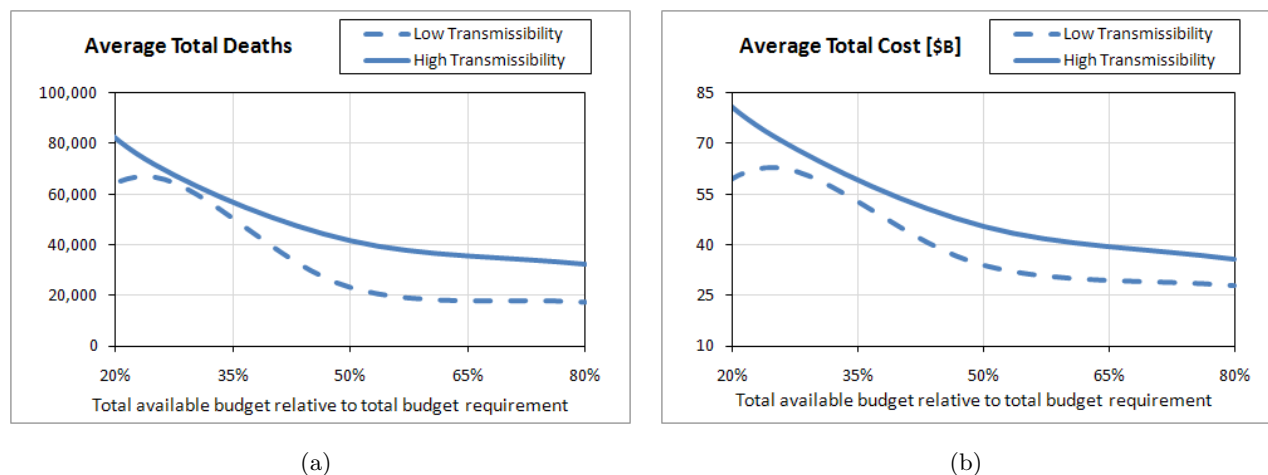


Figure 8: Sensitivity analysis on total budget availability (measured in terms of the average number of deaths (a) and the average total cost (b))

As expected, the curves for the average number of deaths and total cost exhibit a downward trend, for both transmissibility scenarios, as the total budget availability increases. An increased budget translates into higher availabilities of mitigation resources, which will mediate regional pandemic impact and reduce the probability of spread to unaffected regions. As also expected, a higher virus transmissibility generates more infections which, in turn, result into more fatalities and, subsequently, bigger societal and economic costs. As the budget availability approaches the budget requirement (starting from approximately 60%), both impact curves show a converging behavior, for both scenarios, whereby the marginal impact of additional resource availability decreases. This can be explained by noting that the total budget requirement was calculated assuming the worst case scenario where *all* regions are affected and provided with adequate resources to cover their respective populations at risk.

### 4.2.2 Antiviral Efficacy

Figures 9(a) and 9(b) show the behavior of the two impact measures for the level of the antiviral efficacy ( $\tau$  in Eq. 3) between 10% and 20%, and a fixed level of the total budget availability (50% of the the total requirement).

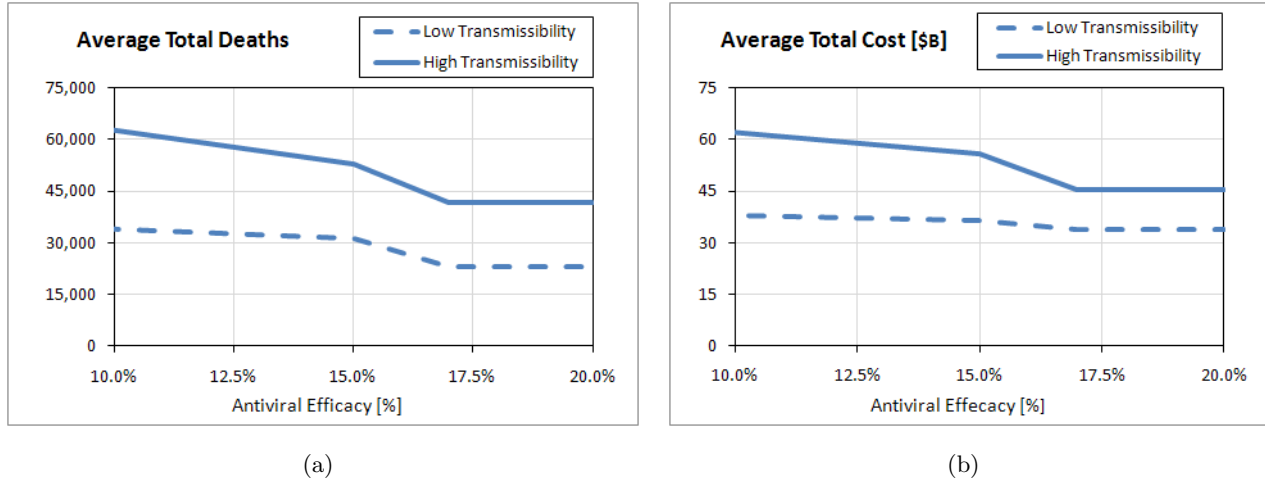


Figure 9: Sensitivity analysis on antiviral efficacy (measured in terms of the average number of deaths (a) and the average total cost (b))

As expected from Eq. 3, for both transmissibility scenarios, the two curves exhibit a decreasing trend which is approximately linear in the range of  $\tau$  between 10% and 15%. As the value of  $\tau$  approaches the value of the maximum base mortality probability (approximately 16% for the elderly risk group), the resultant effective mortality probability tends to zero, which explains the converging behavior of the curve representing the total number of mortalities. The total cost curve exhibits a similar pattern.

### 4.2.3 Vaccine Efficacy

Both impact measure curves exhibit a downward trend as the vaccine efficacy ( $\delta$  in Eq. 6) increases between 20% and 35%, with a fixed level of the total budget availability (50% of the the total require-

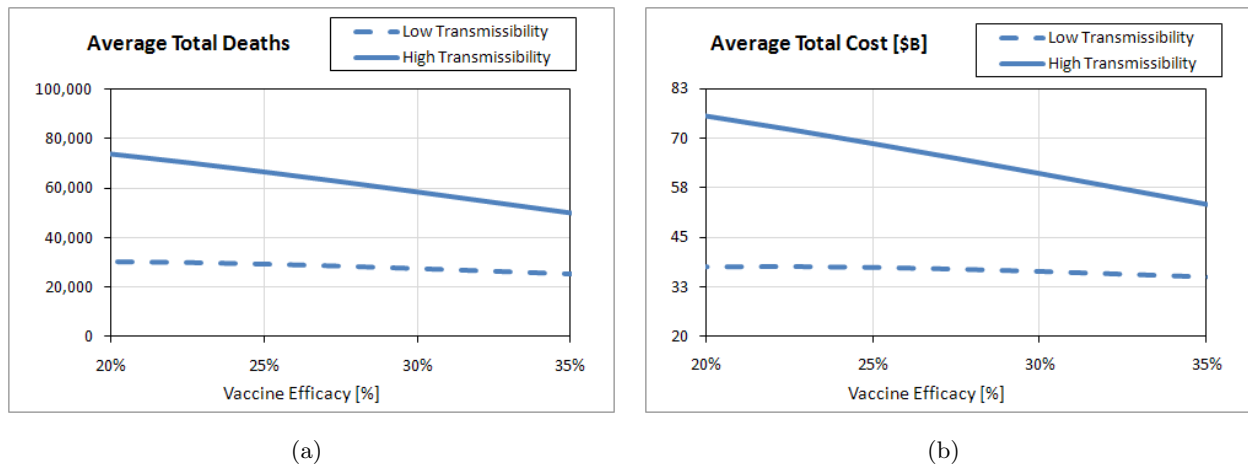


Figure 10: Sensitivity analysis on vaccine efficacy (measured in terms of the average number of deaths (a) and the average total cost (b))

ment) (see Fig. 10(a) and 10(b)). For lower transmissibility, the marginal utility of the vaccine efficacy is less significant which can be explained by noting that such scenarios generate fewer infections and consequently, the overall impact of a more effective vaccine is less pronounced.

#### 4.2.4 Social Distancing Conformance Level

Reduction of the contact intensity through social distancing has long proven to be one of the most efficient mitigation mechanisms. Figures 11(a) and 11(b) show the dynamics of the average number of fatalities and total cost for different levels of the social distancing conformance. The analysis was conducted for conformance levels between 50% and 80%.

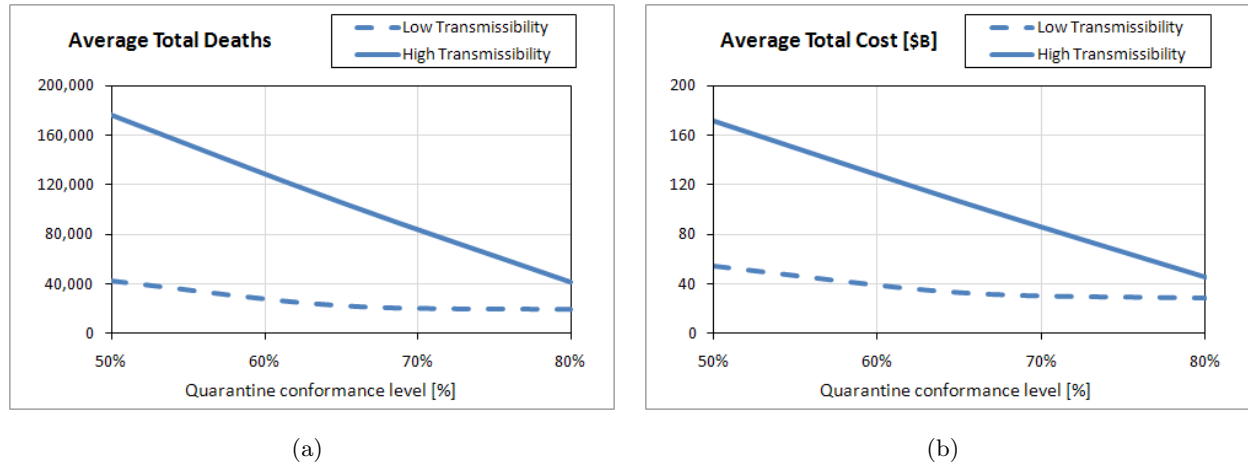


Figure 11: Sensitivity analysis on social distancing conformance (measured in terms of the average number of deaths (a) and the average total cost (b))

For both transmissibility scenarios, the two curves exhibit a downward trend, which can be attributed to a reduced contact intensity associated with higher conformance. The trends are steeper for higher transmissibility scenarios which are characterized by more intensive social dynamics within the mixing groups. The reduction in the contact intensity gets amplified throughout generations of infection within the affected region and, more importantly, leads to reduced probabilities of spread to unaffected regions.

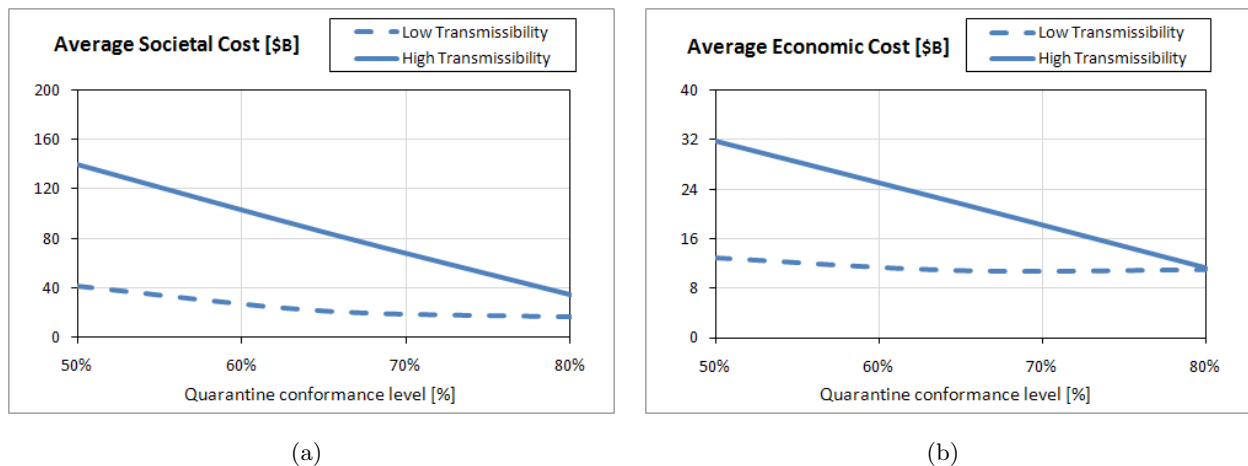


Figure 12: Sensitivity analysis on social distancing conformance (societal (a) and economic cost (b))

Figures 12(a) and 12(b) show the dynamics of the total cost broken into the societal and economic components. The societal cost for the two scenarios generally decreases with quarantine conformance as a consequence of generating fewer infections and deaths (and hence, smaller lost productivity) during the quarantine period. For higher transmissibility, the marginal impact of the conformance level is more pronounced due to the effect of amplifying reduction in contact intensity explained above. A similar behavior can be observed for the economic cost which incorporates the cost of medical expenses of the recovered/deceased (over the entire pandemic period) and the cost of lost productivity of the quarantined individuals (during the social distancing period).

#### 4.2.5 Social Distancing Declaration Threshold

Figures 13(a) and 13(b) show the dynamics of the impact measures for different levels of the social distancing declaration threshold, measured in terms of the CFR (see Section 4.1.3). The analysis was conducted for the CFR values between 0.2% and 1.0%.

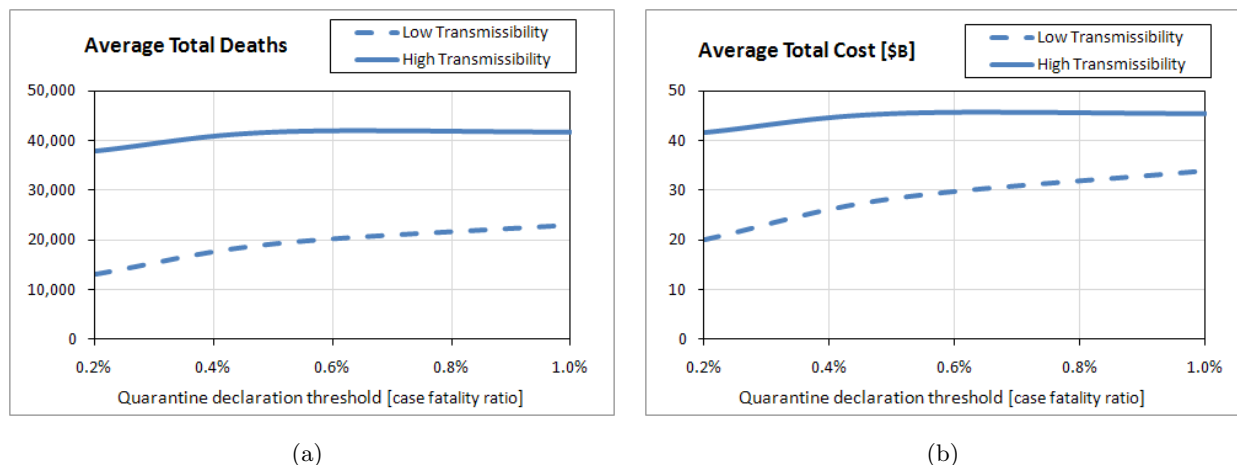


Figure 13: Sensitivity analysis on social distancing declaration threshold (measured in terms of the average number of deaths (a) and the average total cost (b))

For both scenarios, the trends are increasing since later declaration leads to a growth in the number of infected and dead. It can also be observed that for higher transmissibility, the curves reach saturation starting from CFR of approximately 0.55%. This can be explained by noting that in this case, the time difference in quarantine declaration using CFR values between 0.55% and 1.0% is insignificant.

#### 4.2.6 Social Distancing Period

Figures 14(a) and 14(b) show the dynamics of the the average number of fatalities and total cost for different values of the social distancing period (between 10 and 14 days, as recommended by CDC, U.S. [53]). Similar to the analysis for the social distancing conformance level (see Section 4.2.4), for both transmissibility scenarios, the two curves exhibit a decreasing trend: once the case fatality ratio reaches a significant value of 1.0%, social distancing becomes the most efficient containment measure. From this point, any additional quarantine days (starting from 10 and up to 14 total days [53]) will reduce both the contact intensity during the quarantine period and also the size of the post-quarantine infectious population.

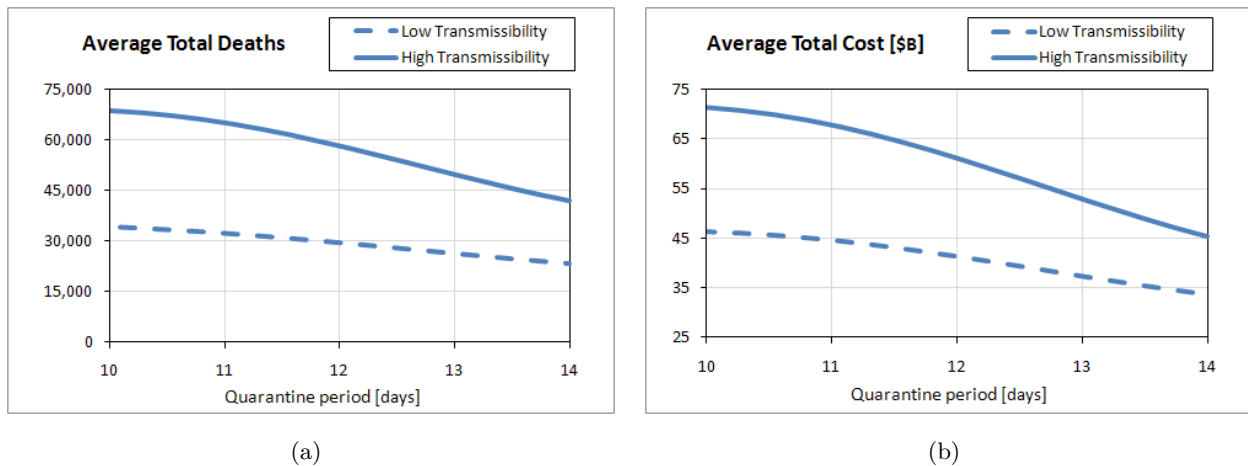


Figure 14: Sensitivity analysis on social distancing period (measured in terms of the average number of deaths (a) and the average total cost (b))

Based on our methodology, we have also developed a decision-aid simulator with a GUI which is made freely available to general public through our web site at <http://imse.eng.usf.edu/pandemics.aspx>. The simulator allows the input of data for regional demographic and social dynamics, and disease related parameters (see Appendix, Fig. 15). It is intended to assist public health decision makers in conducting customized what-if analysis for assessment of mitigation options and development of policy guidelines. Examples of such guidelines include targeted risk groups for vaccination and antiviral treatment, social distancing policies (e.g., thresholds for declaration and lifting, closure options (i.e., household-based, schools, etc.), and compliance targets), and guidelines for travel restrictions.

## 5 Conclusions

Combating influenza pandemics and effectively addressing societal problems entailing such scourges have to invariably rely on understanding the evolution of disease and population dynamics. The practicality and effectiveness of mitigation strategies also significantly depend on available emergency response infrastructure, mitigation resources, and allocation policies. As recently acknowledged by a number of national institutes of health, the existing models for PI mitigation fall short of supporting *dynamic prevention and intervention*, which incorporate a broader spectrum of interventions and measures of societal and economic impact. In this paper, we present a large-scale simulation-based optimization methodology which is specifically aimed at addressing these challenges.

The developed decision-aid methodology incorporates varying virus epidemiology and region-specific population dynamics. The model supports development of mitigation strategies for an efficient, progressive allocation of a limited resource budget over a network of regional outbreaks. The mitigation resources considered in the model included stockpiles of vaccines and antiviral drugs, administration capacities for vaccination and antiviral treatment, and social distancing enforcement resources. Our model seeks to dynamically minimize the impact of ongoing outbreaks and the expected impact of potential outbreaks, spreading from the ongoing regions. The methodology considers measures of morbidity, mortality, and social distancing, translated into the societal and economic costs of lost pro-

ductivity and medical expenses. The methodology was calibrated using historic pandemic data and tested on a sample cross-regional outbreak in Florida, U.S., with over four million people. The paper also presents a sensitivity analysis for estimating the marginal impact (measured in terms of the total pandemic cost and the number of fatalities) of changes in the total budget availability and variability of some critical factors. These factors included vaccine and antiviral efficacy, social distancing declaration threshold, period, and target population conformance. We also examined the impact of social distancing conformance levels of on the dynamics of societal and economic costs.

As our analysis shows, for both transmissibility scenarios, starting with the budget availability of approximately 60% of the total requirement, the marginal impact of additional resources steadily decreases. This can be explained by observing that while the total budget requirement was determined assuming that *all* regions would be affected, our dynamic predictive allocation generally reduces the probability of spread from then ongoing regions, which lessens the actual resource need. Our analysis also suggests that compared to high transmissibility, the marginal utility of the vaccine efficacy for low transmissibility is less significant due to a relatively smaller infected population, which makes the overall impact of a more effective vaccine less pronounced. We have observed that the overall pandemic cost is significantly affected by the social distancing conformance, particularly for higher transmissibility scenarios which are characterized by more intensive social interactions within the mixing groups. The reduction in the contact intensity is amplified throughout generations of infection within the affected region and, more significantly, leads to reduced probabilities of spread to unaffected regions. We have also observed that later declaration of social distancing leads to a growth in the number of infected and dead. Moreover, for both transmissibility scenarios, longer social distancing period (starting from 10 and up to 14 total days [53]) has a significant impact on the pandemic cost by reducing both the contact intensity within the mixing groups and the size of the post-quarantine infectious population.

To the best of our knowledge, the presented methodology is one of the first attempts to offer a *dynamic predictive* decision-aid tool for mitigation of pandemic outbreaks, which incorporates measures of both *societal and economic impact*. Compared to the existing models, such as [47], our study presents the following contributions: (i) our model is capable of re-allocating the resources remaining from the previous distributions, based on the current pandemic status, and thus, achieving a more efficient resource utilization; (ii) our model incorporates the costs of the resources and aims to allocate a total available budget, as opposed to allocating available quantities of individual resources, which vary in their relative cost and effectiveness; (iii) our testbed implementation considered optimal policy generation under both low and high transmissibility scenarios; (iv) finally, our paper attempted to investigate the dynamics of the societal and economic costs under varying social distancing policies. In addition, our simulation represents one of the first of its kind in incorporating a broader range of social behavioral aspects, including vaccination and antiviral treatment conformance of the target population. Our model features a flexible design which can be particularized to an even broader range of pharmaceutical and non-pharmaceutical interventions and more granular mixing groups. The developed methodology is intended to assist public health decision makers in development of dynamic strategies for mitigation of large-scale cross-regional pandemic outbreaks.

## 6 Appendix

Author, year	Single region (SR) / Cross regional (CR)	Model objective	Key features
Ferguson et al, 2005 [44], Ferguson et al, 2006 [14]	SR (Thailand, 2005), SR (U.S. & UK, 2006)	Model PI spread & assess mitigation strategies	<ul style="list-style-type: none"> <li>- 85M Thailand, 300M US, 58.1M UK</li> <li>- Use of GIS (Landscan)</li> <li>- Use of targeted mass prophylaxis and social distancing</li> <li>- A set of homogeneous mixing groups</li> </ul>
Glass et al, 2006 [31]	SR (small town in New Mexico, U.S.)	Examine role of social distancing	<ul style="list-style-type: none"> <li>- Targeted social distancing</li> <li>- Fixed, small-scale contact network</li> <li>- Time between infection events follows an exponential distribution</li> </ul>
Germann et al, 2006 [45]	SR (U.S.)	Assess mitigation strategies	<ul style="list-style-type: none"> <li>- 281M inhabitants (2000 U.S. census data) divided in 2000-person communities</li> <li>- Sensitivity analysis on <math>R_0</math> from 1.6 to 2.4</li> </ul>
Wu et al, 2006 [15]	SR (Hong Kong)	Test different intervention scenarios	<ul style="list-style-type: none"> <li>- Natural history includes pre-symptomatic cases</li> <li>- Use of household-based interventions</li> <li>- Need for significant stocks of antiviral drugs</li> </ul>
Colizza et al, 2007 [24, 93]	CR (global)	Model worldwide spread of a pandemic	<ul style="list-style-type: none"> <li>- Use of an air travel network</li> <li>- Diverse urban centers</li> <li>- Use of compartmental models (SLIR)</li> <li>- Analysis of antiviral and travel restrictions</li> </ul>
Halloran et al, 2008 [49]	SR (Chicago)	Cross-validate targeted layered containment models (Ferguson/Germann/Eubank)	<ul style="list-style-type: none"> <li>- 8.6M people</li> <li>- <math>R_0</math> from 1.9 to 3.0</li> <li>- Assessment of intervention strategies</li> </ul>
Cooley et al, 2007 [94]	SR (North Carolina, U.S.)	Compare a simulated pandemic curve against real-life data	<ul style="list-style-type: none"> <li>- Use of 2003-04 North Carolina data</li> <li>- Use of ILI data to estimate model parameters</li> </ul>
Das, Savachkin & Zhu, 2008 [43]	SR	Mimic stochastic propagation of PI and assess mitigation strategies	<ul style="list-style-type: none"> <li>- Large-scale model (1.1M)</li> <li>- Detailed schedules for inhabitants</li> <li>- Heterogeneous mixing groups</li> </ul>
Savachkin et al, 2009 [47]	CR (Florida, U.S.)	Model PI spread & assess comprehensive dynamic mitigation strategies	<ul style="list-style-type: none"> <li>- Dynamic predictive large-scale simulation-based optimization methodology</li> <li>- 4M people testbed</li> <li>- Use of vaccination, prophylaxes, and social distancing</li> </ul>
STEM-Eclipse, 2009 [95]	CR (global)	Model worldwide PI spread	<ul style="list-style-type: none"> <li>- Geographic visualization of PI spread</li> <li>- Use of SIR model</li> <li>- Limited to land transportation</li> </ul>

Table 1: A summary of simulation-based PI containment and mitigation models

Age Group \ Region	Adult Population Distribution by Age			
	Hillsborough	Miami Dade	Duval	Leon
23 - 29	0.16	0.15	0.16	0.24
30 - 64	0.67	0.66	0.69	0.63
65 - 99	0.17	0.19	0.15	0.13

Table 2: Distribution of regional adult population by age

Age Group \ Region	Children Population Distribution by Age			
	Hillsborough	Miami Dade	Duval	Leon
0 - 5 (pre-school)	0.24	0.22	0.24	0.16
6 - 9 (elementary school)	0.23	0.23	0.25	0.17
10 - 14 (middle school)	0.25	0.25	0.23	0.17
15 - 17 (high school)	0.13	0.14	0.14	0.10
18 - 22 (college)	0.15	0.16	0.14	0.40

Table 3: Distribution of regional children population by age

Household Type		Regional Population by Household Type			
# Adults	# Children	Hillsborough	Miami Dade	Duval	Leon
1	0	0.28	0.25	0.27	0.30
1	1	0.04	0.04	0.04	0.04
2	0	0.31	0.26	0.30	0.32
1	2	0.04	0.05	0.05	0.04
2	1	0.13	0.15	0.14	0.13
1	3	0.01	0.01	0.01	0.01
2	2	0.13	0.15	0.13	0.11
1	4	0.01	0.01	0.01	0.00
2	3	0.06	0.08	0.06	0.04

Table 4: Distribution of regional population by households

Mixing Group (MG) Type	Number of MG	Distribution of Workplaces	Distribution of Weekday Errands	Distribution of Weekend Errands	Distribution of Quarantine Errands	Hourly Contact Rate
Home	1	0.066	0.000	0.000	0.800	1.500
Factory	613	0.058	0.000	0.000	0.000	0.750
Office	2,266	0.302	0.000	0.000	0.000	0.750
Pre-school	224	0.005	0.000	0.000	0.000	1.050
Elementary school	66	0.010	0.000	0.000	0.000	2.573
Middle school	134	0.203	0.000	0.000	0.000	3.750
High school	59	0.097	0.000	0.000	0.000	3.750
College	46	0.106	0.000	0.000	0.000	3.750
Afterschool center	256	0.007	0.000	0.000	0.000	1.500
Grocery store	390	0.026	0.619	0.515	0.100	0.375
Restaurant	223	0.087	0.278	0.256	0.000	0.375
Entertainment center	360	0.032	0.066	0.116	0.000	0.375
Church	86	0.001	0.037	0.113	0.100	0.375

Table 5: Composition of mixing groups, Hillsborough County

Mixing Group (MG) Type	Number of MG	Distribution of Workplaces	Distribution of Weekday Errands	Distribution of Weekend Errands	Distribution of Quarantine Errands	Hourly Contact Rate
Home	1	0.092	0.000	0.000	0.800	1.500
Factory	1,353	0.035	0.000	0.000	0.000	0.750
Office	2,880	0.128	0.000	0.000	0.000	0.750
Pre-school	188	0.010	0.000	0.000	0.000	1.050
Elementary school	246	0.188	0.000	0.000	0.000	2.573
Middle school	84	0.098	0.000	0.000	0.000	3.750
High school	82	0.116	0.000	0.000	0.000	3.750
College	59	0.206	0.000	0.000	0.000	3.750
Afterschool center	507	0.006	0.000	0.000	0.000	1.500
Grocery store	942	0.025	0.619	0.515	0.100	0.375
Restaurant	3,935	0.085	0.278	0.255	0.000	0.375
Entertainment center	758	0.011	0.066	0.116	0.000	0.375
Church	266	0.000	0.037	0.113	0.100	0.375

Table 6: Composition of mixing groups, Miami Dade County

Mixing Group (MG) Type	Number of MG	Distribution of Workplaces	Distribution of Weekday Errands	Distribution of Weekend Errands	Distribution of Quarantine Errands	Hourly Contact Rate
Home	1	0.049	0.000	0.000	0.800	1.500
Factory	519	0.063	0.000	0.000	0.000	0.750
Office	2,880	0.313	0.000	0.000	0.000	0.750
Pre-school	74	0.006	0.000	0.000	0.000	1.050
Elementary school	116	0.170	0.000	0.000	0.000	2.572
Middle school	35	0.083	0.000	0.000	0.000	3.750
High school	30	0.087	0.000	0.000	0.000	3.750
College	21	0.112	0.000	0.000	0.000	3.750
Afterschool center	245	0.006	0.000	0.000	0.000	2.000
Grocery store	320	0.024	0.619	0.515	0.100	1.500
Restaurant	1,474	0.074	0.278	0.255	0.000	0.375
Entertainment center	244	0.012	0.066	0.116	0.000	0.375
Church	77	0.001	0.037	0.113	0.100	0.375

Table 7: Composition of mixing groups, Duval County

Mixing Group (MG) Type	Number of MG	Distribution of Workplaces	Distribution of Weekday Errands	Distribution of Weekend Errands	Distribution of Quarantine Errands	Hourly Contact Rate
Home	1	0.072	0.000	0.000	0.800	1.50
Factory	103	0.012	0.000	0.000	0.000	0.750
Office	1,093	0.212	0.000	0.000	0.000	0.750
Pre-school	20	0.008	0.000	0.000	0.000	1.050
Elementary school	30	0.106	0.000	0.000	0.000	2.573
Middle school	15	0.051	0.000	0.000	0.000	3.750
High school	14	0.064	0.000	0.000	0.000	3.750
College	9	0.374	0.000	0.000	0.000	3.750
Afterschool center	60	0.005	0.000	0.000	0.000	1.500
Grocery store	52	0.021	0.619	0.515	0.100	0.375
Restaurant	512	0.069	0.278	0.255	0.000	0.375
Entertainment center	73	0.006	0.066	0.116	0.000	0.375
Church	16	0.002	0.037	0.113	0.100	0.375

Table 8: Composition of mixing groups, Leon County

Origin \ Destination	Inter-Regional Travel Probability			
	Hillsborough	Miami Dade	Duval	Leon
Hillsborough	0.00	0.60	0.27	0.13
Miami Dade	0.74	0.00	0.16	0.10
Duval	0.61	0.29	0.00	0.10
Leon	0.52	0.31	0.17	0.00

Table 9: Inter-regional travel probabilities

Age Group	0-5	6-19	20-29	31-65	66-99
$\alpha_i$	0.156	0.106	0.205	0.195	0.344

Table 10: Instantaneous infection probability for different age groups

Age Group	% High-Risk Cases	% Death for High-Risk Cases	Mortality Probability
<b>0-19</b>	6.4	9.0	0.007
<b>20-64</b>	14.4	40.9	0.069
<b>65+</b>	40.0	34.4	0.162

Table 11: Mortality probability for different age groups

Mixing group	Hourly contact rate
Home	1.50
Factory	0.75
Office	0.75
Preschool	1.05
Elementary school	2.57
Middle school	3.75
High school	3.75
University	3.75
Afterschool center	1.50
Grocery store	0.38
Restaurant	0.38
Entertainment center	0.38
Church	0.38

Table 12: Hourly contact rates by mixing group (Hillsborough County, high transmissibility scenario)

Region (population)	Resource Requirements by Region					Cost of Resource	Required Budget by Resource
	Hillsb. (1,007,916)	Miami D. (2,209,702)	Duval (852,168)	Leon (248,761)	Total (4,318,547)		
<b>Resource</b>							
Vaccine stock	305,036	679,181	241,522	76,007	1,301,745	\$8.48/dose	\$11,038,800
Antiviral stock	415,294	749,058	460,393	105,307	1,730,052	\$60/dose	\$103,803,140
No. nurses (antiv.)	650	1,104	786	166	2,706	\$27/hr 8 hr/day, 50 days	\$29,226,975
No. nurses (vacc.)	1,059	2,358	839	264	4,520	\$27/hr 8 hr/day, 14 days	\$13,668,326
<b>Total Budget Requirement</b>							<b>\$157,737,241</b>

Table 13: Regional resource and budget requirements

Pandemic Impact Measure (age group, years)	Value US\$
Average cost of lost lifetime productivity of a deceased case (0 - 19)	\$1,336,347.86
Average cost of lost lifetime productivity of a deceased case (20 - 64)	\$1,370,987.28
Average cost of lost lifetime productivity of a deceased case (65 - 99)	\$98,959.24
Average cost of lost productivity and medical expenses of a recovered/deceased case (0 -19)	\$5,078.48
Average cost of lost productivity and medical expenses of a recovered/deceased case (20 -64)	\$10,466.68
Average cost of lost productivity and medical expenses of a recovered/deceased case (65 -99)	\$11,566.09
Average daily cost of lost productivity of a non-infected quarantined case (20-99)	\$432.54

Table 14: Values of pandemic impact measures (societal and economic costs)

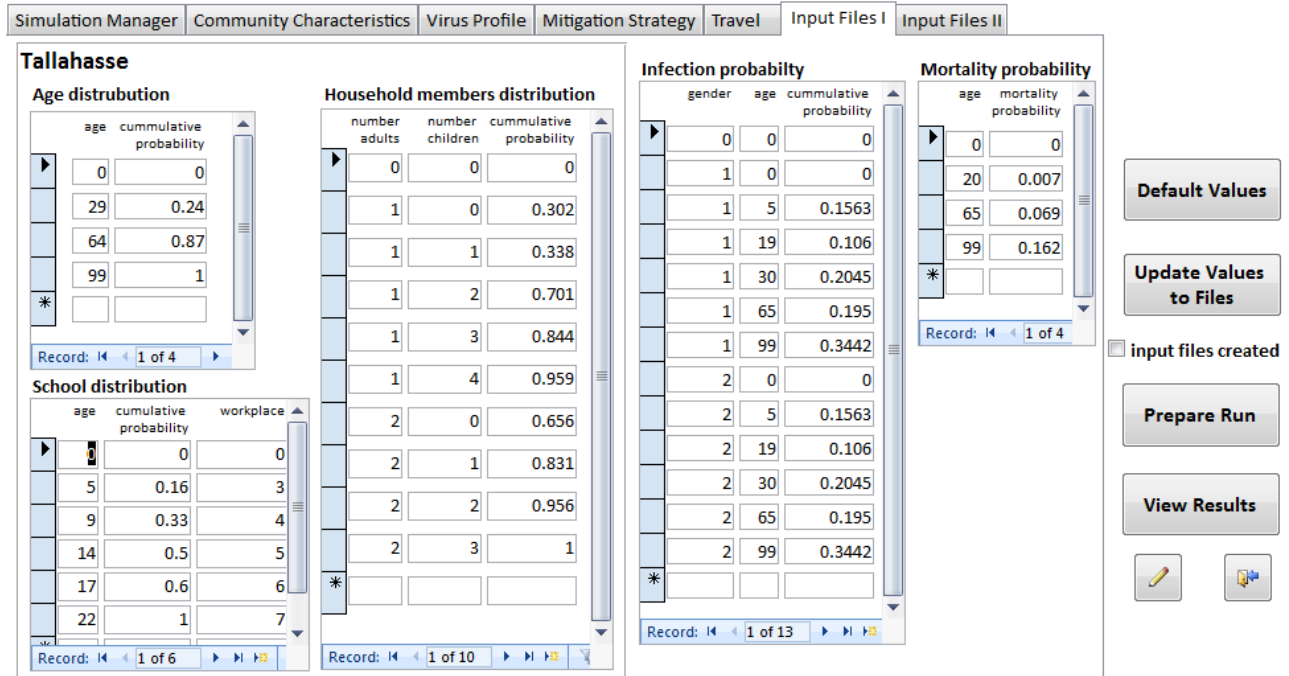


Figure 15: A snapshot of the decision-aid simulator GUI

## References

- [1] Arthur Schoenstadt, “Spanish Flu.” <http://flu.emedtv.com/spanish-flu/spanish-flu.html>, 2009. Last accessed on 12/15/2009.
- [2] I. M. Longini, M. E. Halloran, A. Nizam, and Y. Yang, “Containing pandemic influenza with antiviral agents,” *Am J Epidemiol*, vol. 159, no. 7, pp. 623–633, 2004.
- [3] Centers for Disease Control and Prevention (CDC), “Avian influenza: Current H5N1 situation.” <http://www.cdc.gov/flu/avian/outbreaks/current.htm#clusters>, 2008. Last accessed on 02/09/2008.
- [4] World Health Organization (WHO), “Cumulative number of confirmed human cases of Avian Influenza A(H5N1) reported to WHO.” [http://www.who.int/csr/disease/avian\\_influenza/country/cases\\_table\\_2009\\_12\\_21/en/index.html](http://www.who.int/csr/disease/avian_influenza/country/cases_table_2009_12_21/en/index.html), 2009. Last accessed on 12/21/2009.

- [5] World Health Organization, “Pandemic (H1N1) 2009 - update 80.” [http://www.who.int/csr/don/2009\\_12\\_23/en/index.html](http://www.who.int/csr/don/2009_12_23/en/index.html), 2009. Last accessed on 12/23/2009.
- [6] D. Fedson and S. Hant, “Pandemic influenza and the global vaccine supply,” *Clinical Infectious Diseases*, vol. 36, pp. 1552–1561, 2003.
- [7] J. Aumins, A. Lee, and D. Volkin, *Vaccine production*. Boca Raton: CRC Press LLC, 2 ed., 2000.
- [8] World Health Organization, “Pandemic (h1n1) 2009 vaccine deployment update - 17 december 2009.” [http://www.who.int/csr/disease/swineflu/vaccines/h1n1\\_vaccination\\_deployment\\_update\\_20091217.pdf](http://www.who.int/csr/disease/swineflu/vaccines/h1n1_vaccination_deployment_update_20091217.pdf), 2009.
- [9] WHO Global Influenza Programme, “Pandemic Influenza Preparedness and Response,” tech. rep., World Health Organization, 2009.
- [10] Centers for Disease Control and Prevention (CDC), “Preparing for Pandemic Influenza.” <http://www.cdc.gov/flu/pandemic/preparedness.htm>. Last accessed on 04/27/2009.
- [11] U.S. Department of Health & Human Services, “HHS pandemic influenza plan.” <http://www.hhs.gov/pandemicflu/plan/>, 2007. Last accessed on 03/27/2009.
- [12] R. Larson, “Simple models of influenza progression within a heterogeneous population,” *Operations Research*, vol. 55, no. 399-412, pp. 165–195, 2007.
- [13] M. E. Halloran, I. M. Longini, A. Nizam, and Y. Yang, “Containing bioterrorist smallpox,” *Science*, vol. 298, pp. 1428–1432, 2002.
- [14] N. Ferguson, D. A. Cummings, C. Fraser, J. Cajka, P. C. C., and D. S. Burke, “Strategies for mitigating an influenza pandemic,” *Nature*, vol. 442, no. 27, pp. 448–452, 2006.
- [15] J. T. Wu, S. Riley, C. Fraser, and G. Leung, “Reducing the impact of the next influenza pandemic using household-based public health interventions,” *PLoS Med*, vol. 3, no. 9, pp. 1532–1540, 2006.
- [16] A. Handel, I. Longini, and R. Antia, “Towards a quantitative understanding of the within-host dynamics of influenza A infections,” *Epidemics*, vol. 1, no. 3, pp. 185–195, 2009.
- [17] B. Pourbohloul, A. Ahued, B. Davoudi, R. Meza, L. Meyers, D. Skowronski, I. Villaseñor, F. Galván, P. Cravioto, D. Earn, *et al.*, “Initial human transmission dynamics of the pandemic (H1N1) 2009 virus in North America,” *Influenza Other Respi Viruses*, vol. 3, no. 5, pp. 215–222, 2009.
- [18] M. Atkinson and L. Wein, “Quantifying the Routes of Transmission for Pandemic Influenza,” *Bulletin of Mathematical Biology*, vol. 70, no. 3, pp. 820–867, 2008.
- [19] V. Pitzer, S. Olsen, C. Bergstrom, S. Dowell, and M. Lipsitch, “Little evidence for genetic susceptibility to influenza A (H5N1) from family clustering data,” *Emerg Infect Dis*, vol. 13, no. 7, pp. 1074–1076, 2007.

- [20] V. Pitzer, G. Leung, and M. Lipsitch, “Estimating variability in the transmission of severe acute respiratory syndrome to household contacts in Hong Kong, China,” *American journal of epidemiology*, vol. 166, no. 3, pp. 355–359, 2007.
- [21] Y. Yang, J. Sugimoto, M. Halloran, N. Basta, D. Chao, L. Matrajt, G. Potter, E. Kenah, and I. Longini Jr, “The transmissibility and control of pandemic influenza A (H1N1) virus,” *Science*, vol. 326, no. 5953, pp. 729–733, 2009.
- [22] Y. Yang, M. Halloran, J. Sugimoto, and I. Longini Jr, “Detecting human-to-human transmission of avian influenza A (H5N1),” *Emerg Infect Dis*, vol. 13, no. 9, pp. 1348–1353, 2007.
- [23] S. Cauchemez, F. Carrat, C. Viboud, A. Valleron, and P. Boelle, “A Bayesian (MCMC) approach to study transmission of influenza: application to household longitudinal data,” *Statist. Med.*, vol. 23, pp. 3469–3487, 2004.
- [24] V. Colizza, A. Barrat, M. Barthelemy, and A. Vespignani, “The role of the airline transportation network in the prediction and predictability of global epidemics,” *PNAS*, vol. 103, pp. 2015–2020, 2006.
- [25] J. Epstein, J. Parker, D. Cummings, and R. Hammond, “Coupled contagion dynamics of fear and disease: mathematical and computational explorations,” *PLoS One*, vol. 3, no. 12, 2008.
- [26] J. Epstein, D. Goedecke, F. Yu, R. Morris, D. Wagener, and G. Bobashev, “Controlling pandemic flu: the value of international air travel restrictions,” *PLoS One*, vol. 2, no. 5, 2007.
- [27] M. Halloran, “Invited commentary: Challenges of using contact data to understand acute respiratory disease transmission,” *American Journal of Epidemiology*, vol. 164, no. 10, p. 945, 2006.
- [28] Y. Yang, M. Halloran, and I. Longini Jr, “A Bayesian model for evaluating influenza antiviral efficacy in household studies with asymptomatic infections,” *Biostatistics*, vol. 10, no. 2, p. 390, 2009.
- [29] Y. Tang, I. Longini, and M. Halloran, “Design and evaluation of prophylactic interventions using disease incidence data from close contact groups,” *Applied Statistics*, vol. 55, no. 3, pp. 317–330, 2006.
- [30] D. Scharfstein, M. Halloran, H. Chu, and M. Daniels, “On estimation of vaccine efficacy using validation samples with selection bias,” *Biostatistics*, vol. 7, no. 4, p. 615, 2006.
- [31] R. Glass, W. Beyeler, and H. Min, “Targeted social distancing design for pandemic influenza,” *Emerging Infectious Diseases*, vol. 12, no. 11, pp. 1671–1681, 2006.
- [32] M. Lipsitch, T. Cohen, M. Murray, and B. Levin, “Antiviral resistance and the control of pandemic influenza,” *PLoS Medicine*, vol. 4, no. 1, pp. 111–115, 2007.

- [33] K. R. Nigmatulina and R. C. Larson, “Living with influenza: Impacts of government imposed and voluntarily selected interventions,” *European Journal of Operational Research*, vol. 195, pp. 613–627, 6/1 2009.
- [34] I. M. Longini and J. S. Koopman, “Household and community transmission parameters from final distributions of infections in households.,” *Biometrics*, vol. 38, no. 115-126, 1982.
- [35] I. M. Longini, “The generalized discrete-time epidemic model with immunity: a synthesis,” *Math Biosci*, vol. 82, pp. 19–41, 1986.
- [36] F. Ball and O. Lyne, “Optimal vaccination policies for stochastic epidemics among a population of households,” *Mathematical Biosciences*, vol. 177-178, pp. 333–354, 2002.
- [37] C. Fraser, S. Riley, R. Anderson, N. Ferguson, and R. May, “Factors that make an infectious disease outbreak controllable,” *PNAS*, vol. 101, no. 16, pp. 6146–6151, 2004.
- [38] F. Carrat, A. Lavenu, S. Cauchemez, and S. Delequer, “Repeated influenza vaccination of healthy children and adults: borrow now, pay later?,” *Epidemiol. Infect.*, vol. 134, p. 6370, 2005.
- [39] J. T. Wu, S. Riley, C. Fraser, and G. Leung, “Spatial considerations for the allocation of pre-pandemic influenza vaccination in the United States,” *Proc. R. Soc. Bio. Sci.*, vol. 274, no. 1627, pp. 2811–2817, 2006.
- [40] J. Arino, F. Brauer, P. den Driessche, J. Watmough, and J. Wu, “Simple models for containment of a pandemic,” *J. R. Soc. Interface*, vol. 3, pp. 453–457, 2006.
- [41] C. Dargatz, V. Georgescu, and L. Held, “Stochastic modelling of the spatial spread of influenza in germany,” *Austrian Journal of Statistics*, vol. 35, no. 1, p. 520, 2006.
- [42] N. Ferguson, S. Mallett, H. Jackson, N. Roberts, and P. Ward, “A population-dynamic model for evaluating the potential spread of drug-resistant influenza virus infections during community-based use of antivirals,” *Journal of Antimicrobial Chemotherapy*, vol. 51, pp. 977–990, 2003.
- [43] T. Das, and A. Savachkin, “A large scale simulation model for assessment of societal risk and development of dynamic mitigation strategies,” *IIE Transactions*, vol. 40, no. 9, pp. 893–905, 2008.
- [44] N. M. Ferguson, D. Cummings, S. Cauchemez, C. Fraser, S. Riley, M. Aronrag, S. Lamsirithaworn, and D. Burke, “Strategies for containing an emerging influenza pandemic in Southeast Asia,” *Nature*, vol. 437, pp. 209–214, 2005.
- [45] T. Germann, K. Kadau, I. M. Longini, and C. Macken, “Mitigation strategies for pandemic influenza in the United States,” *PNAS*, vol. 103, pp. 5935–5940, 2006.
- [46] R. Patel, I. Longini, and M. Halloran, “Finding optimal vaccination strategies for pandemic influenza using genetic algorithms,” *Journal of Theoretical Biology*, vol. 234, pp. 201–212, 2005.

- [47] A. Savachkin, A. Uribe, T. Das, and D. Prieto, “Developing dynamic predictive strategies for mitigation of cross-regional pandemic outbreaks,” *IIE Transactions (in review)*, 2009.
- [48] C. Mills, J. Robins, and M. Lipsitch, “Transmissibility of 1918 pandemic influenza,” *Nature*, vol. 432, pp. 904–906, 2004.
- [49] M. E. Halloran, N. M. Ferguson, S. Eubank, and I. Longini, “Modeling targeted layered containment of an influenza pandemic in the United States,” *PNAS*, vol. 105, no. 12, pp. 4639–4644, 2008.
- [50] I. M. Longini, A. Nizam, X. Shufu, K. Ungchusak, W. Hanshaoworakul, D. Cummings, and M. E. Halloran, “Containing pandemic influenza at the source,” *Science*, vol. 309, pp. 1083–1087, 2005.
- [51] S. Eubank, H. Guclu, V. Kumar, M. Marathe, A. Srinivasan, Z. Toroczkai, and N. Wang, “Modelling disease outbreaks in realistic urban social networks,” *Nature*, vol. 429, pp. 180–184, 2004.
- [52] Committee on Modeling Community Containment for Pandemic Influenza, “Modeling community containment for pandemic influenza: A letter report.” <http://www.nap.edu/catalog/11800.html>, 2006. Last accessed on 12/09/2008.
- [53] Centers for Disease Control and Prevention (CDC), “Interim pre-pandemic planning guidance: Community strategy for pandemic influenza mitigation in the United States.” [http://www.pandemicflu.gov/plan/community/community\\_mitigation.pdf](http://www.pandemicflu.gov/plan/community/community_mitigation.pdf), 2007. Last accessed on 04/01/2009.
- [54] HHS, “Pandemic planning update iv,” 2007. <http://www.pandemicflu.gov/plan/panflureport4.html>.
- [55] J. Lawless and J. Lawless, *Statistical models and methods for lifetime data*. Wiley New York, 1982.
- [56] O. Diekmann and J. Heesterbeek, *Mathematical epidemiology of infectious diseases: Model building, analysis and interpretation*. Wiley, 2000.
- [57] M. Bootsma and N. Ferguson, “The effect of public health measures on the 1918 influenza pandemic in the us cities,” *PNAS*, vol. 104, no. 18, pp. 7588–7593, 2007.
- [58] J. Brundage and G. Shanks, “Deaths from bacterial pneumonia during 1918–19 influenza pandemic,” *Emerging Infectious Diseases*, vol. 14, no. 8, p. 1193, 2008.
- [59] Centers for Disease Control and Prevention (CDC), “CDC influenza operational plan.” <http://www.cdc.gov/flu/pandemic/cdcplan.htm>, 2006. Last accessed on 03/27/2009.
- [60] S. Pasteur, “Influenza A(H1N1) 2009 Monovalent Vaccine.” <http://www.fda.gov/downloads/biologicsbloodvaccines/vaccines/approvedproducts/ucm182404.pfd>, 2009. Last accessed on 11/18/2009.
- [61] R. Blendon, L. Koonin, J. Benson, M. Cetron, W. Pollard, E. Mitchell, K. Weldon, and M. Herrmann, “Public response to community mitigation measures for pandemic influenza,” *Emerging Infectious Diseases*, vol. 14, no. 5, p. 778, 2008.

- [62] M. Sadique, W. Edmunds, R. Smith, W. Meerdling, O. de Zwart, J. Brug, and P. Beutels, "Precautionary behavior in response to perceived threat of pandemic influenza," *Emerging Infectious Diseases*, vol. 13, no. 9, p. 1307, 2007.
- [63] R. Maunder, J. Hunter, L. Vincent, J. Bennett, N. Peladeau, M. Leszcz, J. Sadavoy, L. Verhaeghe, R. Steinberg, and T. Mazzulli, "The immediate psychological and occupational impact of the 2003 SARS outbreak in a teaching hospital," *Canadian Medical Association Journal*, vol. 168, no. 10, pp. 1245–1251, 2003.
- [64] E. Robertson, K. Hershenfield, S. Grace, and D. Stewart, "The psychosocial effects of being quarantined following exposure to SARS: a qualitative study of Toronto health care workers," *Canadian Journal of Psychiatry*, vol. 49, pp. 403–407, 2004.
- [65] M. Pearson, C. Bridges, and S. Harper, "Influenza vaccination of health-care personnel," *Recommendations of the Healthcare Infection Control Practices Advisory Committee (HICPAC) and the Advisory Committee on Immunization Practices (ACIP)*[Internet]. Disponible en: [www.cdc.gov/mmwr/preview/mmwrhtml/rr55e209a1.htm](http://www.cdc.gov/mmwr/preview/mmwrhtml/rr55e209a1.htm). Consultado Febrero, 2006.
- [66] M. Keane, M. Walter, B. Patel, S. Moorthy, R. Stevens, K. Bradley, J. Buford, E. Anderson, L. Anderson, and K. Tibbals, "Confidence in vaccination: a parent model," *Vaccine*, vol. 23, no. 19, pp. 2486–2493, 2005.
- [67] V. Niederhauser, G. Baruffi, and R. Heck, "Parental decision-making for the varicella vaccine," *Journal of Pediatric Health Care*, vol. 15, no. 5, pp. 236–243, 2001.
- [68] S. Rhodes and K. Hergenrather, "Exploring hepatitis B vaccination acceptance among young men who have sex with men: facilitators and barriers," *Preventive Medicine*, vol. 35, no. 2, pp. 128–134, 2002.
- [69] S. Rosenthal, R. Kottenhahn, F. Biro, and P. Succop, "Hepatitis B vaccine acceptance among adolescents and their parents," *Journal of Adolescent Health*, vol. 17, no. 4, pp. 248–255, 1995.
- [70] M. Smailbegovic, G. Laing, and H. Bedford, "Why do parents decide against immunization? The effect of health beliefs and health professionals," *Child: Care, Health & Development*, vol. 29, no. 4, p. 303, 2003.
- [71] Colorado Department of Human Services Division of Mental Health, "Pandemic influenza: Quarantine, isolation and social distancing." [http://www.flu.gov/news/colorado\\_toolbox.pdf](http://www.flu.gov/news/colorado_toolbox.pdf). Last accessed on 10/28/2009.
- [72] T. Safranek, D. Lawrence, L. Kuriand, D. Culver, W. Wiederholt, N. Hayner, M. Osterholm, P. O'Brien, and J. Hughes, "Reassessment of the association between Guillain-Barré syndrome and receipt of swine influenza vaccine in 1976-1977: results of a two-state study," *American journal of epidemiology*, vol. 133, no. 9, p. 940, 1991.

- [73] K. Cummings, A. Jette, B. Brock, and D. Haefner, "Psychosocial determinants of immunization behavior in a swine influenza campaign," *Medical Care*, vol. 17, no. 6, pp. 639–649, 1979.
- [74] The New Yorker, "The fear factor." [http://www.newyorker.com/talk/comment/2009/10/12/091012taco\\_talk\\_specter](http://www.newyorker.com/talk/comment/2009/10/12/091012taco_talk_specter). Last accessed on 10/28/2009.
- [75] The New York Times, "Doctors swamped by swine flu vaccine fears." [http://www.msnbc.msn.com/id/33179695/ns/health-swine\\_flu/](http://www.msnbc.msn.com/id/33179695/ns/health-swine_flu/). Last accessed on 10/28/2009.
- [76] U.S Census Bureau, "2001 American community survey." <http://www.census.gov/prod/2001pubs/statab/sec01.pdf>, 2000. Last accessed on 03/27/2009.
- [77] Bureau of transportation statistics, "2001 National household travel survey (NTHS)." [http://www.bts.gov/programs/national\\_household\\_travel\\_survey/](http://www.bts.gov/programs/national_household_travel_survey/), 2002. Last accessed on 12/09/2008.
- [78] Tampa International Airport, "Daily schedule." <http://www.tampaairport.com/>, 2008. Last accessed on 12/09/2008.
- [79] "Miami international airport." <http://www.miami-airport.com/>. Last accessed on 12/09/2008.
- [80] Jacksonville Aviation Authority, "Daily schedule." <http://www.jaa.aero/General/Default.aspx>, 2008. Last accessed on 12/09/2008.
- [81] Tallahassee Regional Airport, "Daily schedule." <http://www.talgov.com/airport/index.cfm>, 2008. Last accessed on 12/09/2008.
- [82] Writing committee of the World Health Organization (WHO), "Consultation on human influenza A/H5. Avian influenza A(H5N1) infection in humans," *N Engl J Med*, vol. 353, no. 13, pp. 1374–1385, 2005.
- [83] M. Meltzer, N. Cox, and K. Fukuda, "The economic impact of pandemic influenza in the United States: Priorities for intervention," *Emerging Infectious Diseases*, vol. 5, no. 5, pp. 659–671, 1999.
- [84] World Health Organization (WHO), "WHO guidelines on the use of vaccine and antivirals during influenza pandemics." [http://www.who.int/csr/resources/publications/influenza/11\\_29\\_01\\_A.pdf](http://www.who.int/csr/resources/publications/influenza/11_29_01_A.pdf), 2004. Retrieved 03/27/2009.
- [85] Institute of Medicine (IOM), "Antivirals for pandemic influenza: Guidance on developing a distribution and dispensing program," *The National Academies Press*, 2008.
- [86] J. Treanor, J. Campbell, K. Zangwill, T. Rowe, and M. Wolff, "Safety and immunogenicity of an inactivated subvirion influenza A(H5N1) vaccine," *N Engl J Med*, vol. 355, no. 13, p. 1343, 2006.
- [87] PayScale. <http://www.payscale.com/rcsearch.aspx?country=US&str=Registered+Nurse+>. Last accessed on 12/28/2009.

- [88] Centers for Disease Control and Prevention. <http://www.cdc.gov/vaccines/programs/vfc/cdc-vac-price-list.htm#flu>. Last accessed on 12/28/2009.
- [89] Centers for Disease Control and Prevention. <http://www.pharmacychecker.com/Pricing.asp?DrugId=36260&DrugStrengthId=61300&sortBy=Price>. Last accessed on 12/28/2009.
- [90] R. Blendon, C. DesRoches, M. Cetron, J. Benson, T. Meinhardt, and W. Pollard, "Attitudes toward the use of quarantine in a public health emergency in four countries," *Health Affairs*, vol. 25, no. 2, pp. 15–25, 2006.
- [91] A. Svensson, "A note on generation times in epidemic models," *Math Biosci*, vol. 208, no. 1, pp. 300–311, 2007.
- [92] T. Halfhill, "Inflation calculator." <http://www.halfhill.com/inflatation.html>, 2009. Last accessed on 12/04/2009.
- [93] V. Colizza, A. Barrat, A. V. M. Barthelemy, and A. Vespignani, "Modeling the worldwide spread of pandemic influenza: baseline case and containment interventions," *PLOS Medicine*, vol. 4, pp. 95–110, 2007.
- [94] P. Cooley, L. Ganapathi, G. Ghneim, S. Holmberg, W. Wheaton, and C. Hollingsworth, "Using influenza-like illness data to reconstruct an influenza outbreak," *Mathematical and Computer Modelling*, no. 48, pp. 929–939, 2008.
- [95] F. Eclipse, "The Spatio-Temporal Epidemiological Modeler." <http://www.eclipse.org/stem/intro.php>, 2009. Last accessed on 11/06/2009.